Progress In Electromagnetics Research B, Vol. 26, 179–212, 2010

MULTIPOLE EXPANSION OF ELECTROMAGNETIC SCATTERING WAVE BY A SMALL CYLINDRICAL PORE ON A PERFECT CONDUCTING SEMI-INFINITE HALF SPACE

C. Y. Kuo

Division of Mechanics
Research Center for Applied Sciences, Academia Sinica
128, Nankang 115, Taipei, Taiwan

R. L. Chern and C. C. Chang

Institute of Applied Mechanics
National Taiwan University
1, Section 4, Roosevelt Road, Taipei 106, Taiwan

Abstract—The scattering of an oblique electromagnetic wave incident on a sub-wavelength circular pore with a finite depth on the surface of a semi-infinite perfect conductor is investigated analytically. We use the method of matched asymptotic expansion to find the multipole structure. The expansion is based on the duality property of the source-free Maxwell equations, and the resultant scattering fields are fully expressed in terms of the scalar and the conjugate vector potentials. There are two regions defined by the analytical method: the electro/magneto-static inner region and the radiation outer wave region. For both TM and TE incidences, the scattering waves are lead by leading dipoles. In the next order of the scattering waves, a mixture of the dipole, the quadrupole and the octupole is found. This is a striking finding, that the multipoles are not organized in a strictly ascending manner when the size of the pore is considered. In addition, the sophisticated three-dimensional interplay of the multipoles, the pore depth, and the incident angle is revealed. The magnitudes of the scattering dipoles are confirmed convergent smoothly to those of the back-scattering dipoles of electromagnetic waves transmitted through a hole in a perfect conducting plate with a finite thickness when the pore depth is larger than about 1, normalize to the pore radius.

Received 30 June 2010, Accepted 17 September 2010, Scheduled 15 October 2010
Corresponding author: C. Y. Kuo (cykuo06@gate.sinica.edu.tw).

1. INTRODUCTION

The aim of this paper is to investigate analytically the scattering of electromagnetic waves incident on a small circular pore with a finite depth in a semi-infinite perfect conducting surface. The radius and the pore depth are both assumed to be much smaller than the wavelength of the incident waves. Under such circumstances, a multipole expansion is appropriate for understanding both the electromagnetic fields in the near field around the pore and their incurred radiation in the outer region. The method of matched asymptotic expansion is often used for this purpose. In the method, the entire wave propagation domain is divided into two regions according to their characteristic length scales: the inner electro/magnetic-static region, for the area near/in the pore; and the outer region, for the wave radiation.

Our motivation began with the renewed interests in electromagnetic waves incident on flat surfaces with designed structures of small pores. For example, Pendry et al. [1] demonstrated that a perfect conducting surface with a periodic groove structure mimics the surface plasmon effects. Subsequently, Garcia de Abajo and Saenz [2] calculated the effective permittivity of a flat perfect conductor with such a pore structure to model surface plasmon on metal surfaces and pointed out that the TM waveguide modes in the pore are substantial.

The surface wave of the structured surface can be formulated by the interaction of the scattering waves between pores [3], i.e., the multiple scattering theory. This method eliminates the difficulties of numerical field solvers with slow convergence of the radiation waves at infinity. The milestone for this approach is the thorough understanding of the wave scattering mechanism of an individual aperture (pore). The leading scattering term of a single pore is undoubtedly a dipole. Garcia de Abajo [4] found the leading dipole strength elegantly on the energy flux conservation, and Garcia-Vidal et al. [5] further investigated the transmission of the wave through a single rectangular hole in a perfect conductor plate using the finite-difference time-domain (FDTD) numerical scheme.

Along the line of development for the multiple scattering theory of tailored surfaces, we need an expansion that is able to incorporate the mutual interactions among pores. These additional modifications are expected with the influences of the higher order multipoles. This intrigues us to derive analytically a multipole expansion with the oblique incident effect to complement the understanding of the single pore scattering.

It is well known that when scattering obstacles are small compared

to the wavelengths of the incident waves, the leading order of the near field exhibits electro/magneto-static behavior, [5–7]. For convenience, the static fields are solved with the help of scalar Laplacian potentials [8, 9]. However, due to the coupling between the electric and magnetic fields, far fewer investigations are carried further to the radiation of the electromagnetic fields. Hansen and Yaghjian [10] calculated the leading radiation from small two-dimensional scatterers of arbitrary shapes, either a bump or a dent in/on a ground perfect conducting plane. The effect of the scatterers were formulated into integral equations of the surface current. Then the leading scattering terms were related to the integration of the surface current expansion. Scharstein and Davis [11] further carried out the electromagnetic wave scattering of a two-dimensional sub-wavelength semi-circular trough in a ground plane. The method of matched asymptotic expansion was applied to solve the multipole structure of the scattering wave to the fourth order. Although a multipole expansion is derived, the two-dimensional wave is different from the current interest of the three-dimensional problem. The main difference is that the former is of the cylindrical wave type, but the latter is of the spherical one. In addition, the scattering waves have dependencies on both of the spherical azimuthal and colatitude angles, which are associated with the spherical harmonics. A rich multipole structure, hence, can be generated when the incident wave sheds obliquely on the pore.

Extensive theoretical work for the electromagnetic wave scattering by various aperture structures in conducting screens was done in the 70s to 80s, see [12–14] and references therein. Most of the theories were developed by matching the tangential components of the physical fields (electric or magnetic) at the joint plane of the aperture and the radiation domain. Closely related to the current work, Roberts [14, 15] developed a rigorous method for the scattering from a circular aperture in a perfect conducting plate with a finite thickness. Thorough calculations were performed for wide ranges of incident angles and incident wavenumbers. Physical fields of the near-field region were also demonstrated, and rich patterns of scattering directivities were found for large wavenumber incidence. On the other hand, explicit forms for the scattering can be made with classical multipole expansions for small scatterers or pores. High order accuracy of the scattering wave can be obtained by expansions involving polynomial series of the wave number: Rayleigh series. Various procedures have been developed. For example, Stenvenson [6] formulated a set of integro-differential equations for magnetic currents in the series and solved for scattering due to apertures of elliptic/circular shapes in infinitely thin plates.

In principle, the general purpose theories are applicable to our

present problem, with additional accounting for a waveguide section connecting to the pore. One way to incorporate the long wavelength assumption with the aforementioned wave scattering theory is to find the asymptotic expansion by directly manipulating the spherical harmonic functions. However, for providing an alternative physical intuition, we formulate the potentials using the duality property of the source-free Maxwell equations — a scalar electric potential and its associated magnetic vector potential and vice versa. The Lorentz gauge condition is used to solve the potentials. Use of this gauge condition also avoids the ambiguity of the Coulomb gauge, whose potential is instantly seen in the propagation field without the retarded time of wave propagation [16].

For the same geometric configuration, Kuo et al. [17] use the method of matched asymptotic expansion to solve the acoustic scattering problem. Scalar variables, the pressure perturbations in different orders of magnitude, are the primary physical variables. Both rigid and pressure-release boundary conditions are solved. In this paper, we will show that the scalar variables are related to the scalar potentials in the electromagnetic waves. Hence, their method of solution can be extensively applied herein, and analogous comparison between the two systems is made.

In what follows, we describe the geometry of the problem and the duality formulation of the source-free Maxwell equations in Section 2. The scattering of the TM incidence and the TE incidence are solved in Sections 3 and 4, respectively. The main results, the radiation multipole structure of the potentials are tabulated in Tables 1, 2, and 3.

2. GEOMETRY AND GOVERNING EQUATIONS

The problem of interest is sketched in Fig. 1. There is a circular pore with a finite depth drilled in a semi-infinite perfect conducting bulk domain. The pore has a radius a^* and a finite depth ℓ^*. We assume that ℓ^* and a^* are comparable in the present paper; i.e., both are much smaller than the wavelength of the incident wave. Without loss of generality, we choose the x-axis of the Cartesian coordinate in alignment with the horizontal projection of the propagation vector $\mathbf{k}^*$; that is, its y-component, k_y^*, is zero and the incident electromagnetic plane wave is directed to the pore with an incident angle α.

The source-free Maxwell equations with a time harmonic proportional to $\exp(-i\omega^* t^*)$ are

$$\begin{aligned} &\nabla^* \cdot \mathbf{E}^* = 0, \quad \nabla^* \times \mathbf{E}^* = i\omega^* \mathbf{B}^*, \\ &\nabla^* \cdot \mathbf{B}^* = 0, \quad \nabla^* \times \mathbf{B}^* = -\frac{i\omega^*}{c^{*2}} \mathbf{E}^*, \end{aligned} \tag{1}$$

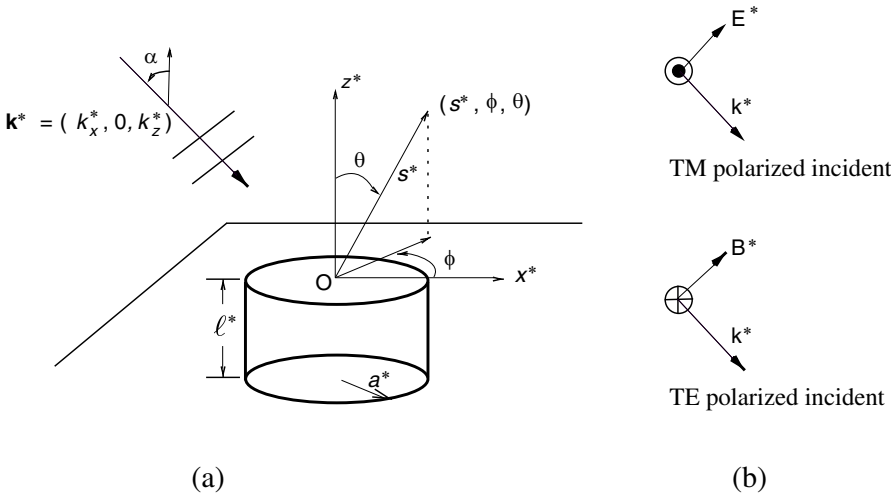

Figure 1. (a) The coordinate system and the incident wave and (b) the polarization definition of the incident wave.

where $\mathbf{E}^*$ and $\mathbf{B}^*$ are the electric and magnetic fields and c^* is the light speed in vacuum. Variables with an asterisk superscript * denote the dimensional physical quantities.

The electric and magnetic fields are mutually coupled in these equations. However, the solution process for analytical solutions is made possible by introducing auxiliary potentials. Defining the magnetic vector potential

$$\mathbf{B}^* = \nabla^* \times \mathbf{A}_M^*, \tag{2}$$

and substituting into $(1)_2$, we obtain an accompanying scalar potential Ψ_E^*, such that

$$\mathbf{E}^* = i\omega^* \mathbf{A}_M^* + \nabla^* \Psi_E^*. \tag{3}$$

Choosing the Lorentz gauge condition,

$$\nabla^* \cdot \mathbf{A}_M^* + \frac{i\omega^*}{c^{*2}} \Psi_E^* = 0, \tag{4}$$

both of the potentials satisfy the wave equations

$$\nabla^{*2} \Psi_E^* + k^{*2} \Psi_E^* = 0, \text{ and } \nabla^{*2} \mathbf{A}_M^* + k^{*2} \mathbf{A}_M^* = 0. \tag{5}$$

On the other hand, because of the symmetric form of the Maxwell equations, we can define a set of dual potentials $\mathbf{A}_E^*$ and Ψ_M^*, such that

$$\mathbf{E}^* = -\nabla^* \times \mathbf{A}_E^*, \text{ and } \mathbf{B}^* = \frac{i\omega^*}{c^{*2}} \mathbf{A}_E^* + \nabla^* \Psi_M^*. \tag{6}$$

Similarly, the potentials satisfy the wave equations

$$\nabla^{*2}\Psi_M^* + k^{*2}\Psi_M^* = 0, \text{ and } \nabla^{*2}\mathbf{A}_E^* + k^{*2}\mathbf{A}_E^* = 0, \tag{7}$$

under the gauge condition

$$\nabla^* \cdot \mathbf{A}_E^* + i\omega^*\Psi_M^* = 0. \tag{8}$$

Equations (4), (5), (7) and (8) are now our system of governing equations, and the physical fields are calculated with (2), (3) and (6).

The scattering potential is induced by the geometrical non-uniformity of the pore. Since its length scale is the pore radius, the potentials are nondimensionalized as

$$\mathbf{A}_M = \frac{c^*}{2|E_{inc}^*|a^*}\mathbf{A}_M^*, \quad \Psi_M = \frac{c^*}{2|E_{inc}^*|a^*}\Psi_M^*,$$

and

$$\mathbf{A}_E = \frac{1}{2|E_{inc}^*|a^*}\mathbf{A}_E^*, \quad \Psi_E = \frac{1}{2|E_{inc}^*|a^*}\Psi_E^*,$$

where $2|E_{inc}^*|$ is twice the electric amplitude of the incident wave.

In application of the method of matched asymptotic expansion, the domain of interest is conceptually divided into the inner and outer regions, which correspond to the near and far fields with respect to the hole position, see Fig. 2. The inner and outer coordinates are characterized by the hole radius a^* and the wavelength $\lambda^* = 2\pi/k^*$, respectively. The condition that the hole size is much smaller than the wavelength gives rise to a small parameter $\epsilon \equiv k^*a^* \ll 1$, defined as the product of wave number and hole radius. By use of the perturbation technique, the physical quantity is expanded as series of ϵ, and the equations are derived by collecting the series terms for each order of ϵ.

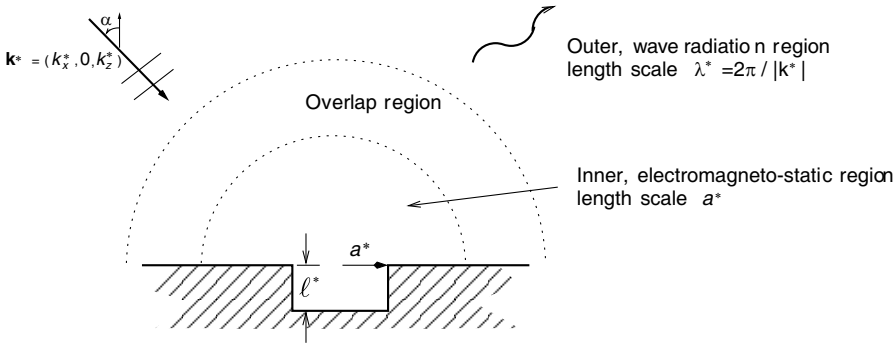

Figure 2. The concept of the matched asymptotic expansion.

In the inner region, the governing equations are shown to be the Laplace equation for the leading-order and the Poisson equation for the second-order, c.f. $(11)_{1,2}$. This is to say that both electric and magnetic fields are quasistatic in the inner region. Inside the hole, the solutions are expressed as a sum of waveguide modes. The Fabrikant theory [18] is used to recast the integral representation for the scattered fields into analytical functions. Continuity of the electric and magnetic fields at the hole exits gives the boundary conditions for solving the weighted coefficients of the waveguide modes and, thus, the near-field solutions are determined accordingly. On the other hand, the fields in the outer region are radiative and are described by the Helmholtz equation, c.f. $(9)_{1,2}$. The far-field solutions are expanded into series of spherical harmonics. The principle of asymptotic matching ensures that there exists an overlap region between the inner and outer fields where the asymptotic representation of the inner solution (at the far-field limit) be identical to that of the outer solution (at the near-field limit) [17, 19]. By matching this condition, the weighted coefficients of spherical harmonics and the far-field solutions are obtained and the inner, outer, and hole solutions are combined together to give the whole solutions of the underlying problem.

On the previous outline of the matched asymptotic expansion, we normalize (1) and (5) with respect to the wave length to find the equations for the outer radiative region:

$$\left(\nabla_o^2 + 1\right)\mathbf{A}_{M,E} = \mathbf{0},\ \left(\nabla_o^2 + 1\right)\Psi_{M,E} = 0,\ \nabla_o \cdot \mathbf{A}_{M,E} = -i\Psi_{E,M}, \quad (9)$$

where subscript $_o$ stands for the outer region. The physical electro/magnetic fields, (3) and (6), in the region are, thus

$$\mathbf{B} = i\epsilon\mathbf{A}_E + \epsilon\nabla_o\Psi_M,\ \mathbf{E} = i\epsilon\mathbf{A}_M + \epsilon\nabla_o\Psi_E. \quad (10)$$

On the other hand, normalization against the pore radius leads to the equations for the inner region:

$$\left(\nabla_i^2+\epsilon^2\right)\mathbf{A}_{M,E} = \mathbf{0},\ \left(\nabla_i^2+\epsilon^2\right)\Psi_{M,E} = 0,\ \nabla_i\cdot\mathbf{A}_{M,E} = -i\epsilon\Psi_{E,M}, \quad (11)$$

where ϵ is the product of k^* and a^*, the small parameter. The subscript $_i$ stands for the inner region. The physical fields in the inner region are, consequently,

$$\mathbf{B} = i\epsilon\mathbf{A}_E + \nabla_i\Psi_M,\ \mathbf{E} = i\epsilon\mathbf{A}_M + \nabla_i\Psi_E. \quad (12)$$

To construct the solutions, we expand the potentials by $\mathbf{A}_{M,E} = \mathbf{A}^{(0)}_{M,E} + \epsilon\mathbf{A}^{(1)}_{M,E} + \epsilon^2\mathbf{A}^{(2)}_{M,E} + O(\epsilon^3)$ and $\Psi_{M,E} = \Psi^{(0)}_{M,E} + \epsilon\Psi^{(1)}_{M,E} + \epsilon^2\Psi^{(2)}_{M,E} + O(\epsilon^3)$ into (11), with the bracketed superscript indicating the magnitude order of the solution terms. The scattering field is induced in respond to the incident wave and, therefore, we need to determine the expansion series and define the polarization of the incident wave to start the matching procedures.

3. TRANSVERSE MAGNETIC POLARIZED INCIDENCE

3.1. External Wave Field

The coordinate system is sketched in Fig. 1. Furthermore, we adopt the polarization definition as in the waveguide theory, i.e., $B_z = 0$ for TM mode in the pore. Under this coordinate system and the polarization definition, the only non-vanishing magnetic component of the TM incident wave is B_y^*. The solution to this polarized incident wave will be presented in this section. On the other hand, there exist two non-zero magnetic components, B_x^* and B_z^*, in the TE polarized incident configuration, and its incurred scattering field will be shown in Section 4.

Now, we have the TM polarized external wave field, the sum of the incident wave with its total reflective wave by the flat infinite perfect conducting surface

$$\mathbf{B}_{ext}^* = 2\frac{|E_{inc}^*|}{c^*}\begin{pmatrix} 0 \\ 1 \\ 0 \end{pmatrix}\exp(ik_x^* x^*)\cos(k_z^* z^*),$$

and

$$\mathbf{E}_{ext}^* = 2i|E_{inc}^*|\begin{pmatrix} k_z^*\sin(k_z^* z^*) \\ 0 \\ ik_x^*\cos(k_z^* z^*) \end{pmatrix}\exp(ik_x^* x^*),$$

where the suffix $_{ext}$ represents the external field. We use the bracket vector forms for the Cartesian component unless otherwise stated.

Near the pore exit, we nondimensionalize the external wave field and express it in an asymptotic series with the inner spatial coordinate

$$\mathbf{B}_{ext} = \begin{pmatrix} 0 \\ 1 \\ 0 \end{pmatrix}(1 + i\epsilon k_x x) + O(\epsilon^2), \tag{13}$$

and

$$\mathbf{E}_{ext} = -k_x\begin{pmatrix} 0 \\ 0 \\ 1 \end{pmatrix} + i\epsilon\begin{pmatrix} k_z^2 z \\ 0 \\ -k_x^2 x \end{pmatrix} + O(\epsilon^2), \tag{14}$$

where $k_x = \sin\alpha$ and $k_z = \cos\alpha$.

To match the field in the pore, it is convenient to recast (13) and (14) into the dual potentials. They are

$$\begin{aligned}\mathbf{B}_{ext} &= \nabla_i(\rho\sin\phi) + i\epsilon k_x\nabla_i \times \left(\mathbf{e}_\rho\frac{\rho z}{2}\right) + \frac{i\epsilon k_x}{4}\nabla_i\left(\rho^2\sin(2\phi)\right) + O(\epsilon^2) \\ &= \nabla_i\Psi_{M,ext}^{(0)} + \nabla_i \times \mathrm{A}_{M,ext}^{(1)} + \nabla_i\Psi_{M,ext}^{(1)} + O(\epsilon^2),\end{aligned} \tag{15}$$

and

$$\begin{aligned}\mathbf{E}_{ext} &= -k_x\nabla_i z + i\epsilon\nabla_i \times (\mathbf{e}_z\rho z\sin\phi) - i\epsilon k_x^2\nabla_i(\rho z\cos\phi) + O(\epsilon^2)\\ &= \nabla_i\Psi^{(0)}_{E,ext} + \nabla_i \times \mathrm{A}^{(1)}_{E,ext} + \nabla_i\Psi^{(1)}_{E,ext} + O(\epsilon^2), \qquad (16)\end{aligned}$$

where $\mathbf{e}_\rho$ and $\mathbf{e}_z$ are the unit vectors in the ρ and z axes of the cylindrical coordinates, (ρ, ϕ, z). The subscript $_{ext}$ denotes the external incident field. One can easily check that the potentials satisfy the gauge condition, $(11)_3$ in the inner region. These external fields provide the forcing fields to produce the scattering wave when a small pore is present at the origin.

3.2. Scalar Potentials and Their Radiation

The scalar potentials in the external field, in the first and the third terms of (15), and (16), suggest that the contribution of the inner potentials reads

$$\mathbf{B}^{(0,1)} = \nabla_i\Psi^{(0,1)}_M, \qquad \mathbf{E}^{(0,1)} = \nabla_i\Psi^{(0,1)}_E,$$

where the bracketed superscripts, $^{(0,1)}$ indicate the first two orders of the magnitude in ϵ of their physical variables. For the perfect conducting surface, we have $\Psi^{(0,1)}_E = 0$, the Dirichlet condition, and $\partial\Psi^{(0,1)}_M/\partial n = 0$, the Neumann condition, on the boundaries for the vanishing surface electric components and the vanishing normal magnetic component, respectively. Both the electric and magnetic scalar potentials satisfy the Laplace equation. In this section, we will solve accordingly the magnetic and electric scalar potentials.

We start from the magnetic potential. Because this potential satisfies the Neumann boundary condition on the perfect conducting surface, the equation for the potential is similar to the acoustic scattering with the rigid condition. We have the integral equation to relate the scattering magnetic scalar potentials $\Psi^{(0,1)}_{M,sc}$, the external forcing potential $\Psi^{(0,1)}_{M,ext}$, and the potential in the pore $\Psi^{(0,1)}_{M,pore}$ at the pore exit plane, $0 \le \rho < 1,\ z = 0$,

$$\begin{aligned}&\Psi^{(0,1)}_{M,pore}|^{<}\\ =&\Psi^{(0,1)}_{M,ext}|^{<} - \frac{1}{2\pi}\int_0^{2\pi}\int_0^1 \frac{\partial\Psi^{(0,1)}_{M,sc}}{\partial z_0}\Big|^{<} \frac{\rho_0 d\rho_0 d\phi_0}{\sqrt{\rho^2+\rho_0^2-2\rho\rho_0\cos(\phi-\phi_0)}}. \qquad (17)\end{aligned}$$

The external potentials are $\Psi^{(0)}_{M,ext} = \rho\sin\phi$ and $\Psi^{(1)}_{M,ext} = ik_x\rho^2\sin(2\phi)/4$, defined in the first and third terms of (15). The

subscripts, $_{sc}$ and $_{pore}$, refer to the scattering and the total potential in the pore. The evaluation symbol, $|^{<}$, stands for the fact that its operand is evaluated on the area $\rho \leq 1$ at $z = 0$.

This integral equation, (17), is a Fredholm integral equations of the first kind. By satisfying this equation, the resultant potential field in the semi-infinute domain $z \geq 0$ is

$$\Psi_M^{(0,1)} = \Psi_{M,ext}^{(0,1)} + \Psi_{M,sc}^{(0,1)}, \tag{18}$$

and the potential in the pore $z < 0$ is

$$\Psi_M^{(0,1)} = \Psi_{M,pore}^{(0,1)}, \tag{19}$$

and the potential is smoothly continuous across the pore exit. In the following, we will describe the essential details related to the present electromagnetic wave scattering but defer the derivation and inversion procedures to Fabrikant [18] and Kuo et al. [17].

The magnetic potentials for $O(\epsilon^0)$ and $O(\epsilon)$ in the pore can be expanded by the infinute sum of the eigen-solutions

$$\begin{aligned}
\Psi_{M,pore}^{(0)}(\rho,\phi,z) &= \bar{A}_{M,1n}^{(0)} J_1(j'_{1n}\rho)\sin\phi \frac{\cosh(j'_{1n}(z+\ell))}{\cosh(j'_{1n}\ell)}, \\
\Psi_{M,pore}^{(1)}(\rho,\phi,z) &= ik_x \bar{A}_{M,2n}^{(1)} J_2(j'_{2n}\rho)\sin(2\phi) \frac{\cosh(j'_{2n}(z+\ell))}{\cosh(j'_{2n}\ell)},
\end{aligned} \tag{20}$$

where j'_{mn} is given by $J'_m(j'_{mn}) = 0$. The summation symbol that represents summing over from $n = 1$ to ∞ is omitted. The system equations are similar to the first- and the second-order equations of the acoustic equations for the rigid condition, (6) and (19), with only $m = 2$, of [17], except that the acoustic incident wave ik_x, $-k_x^2$ is replaced by 1 and ik_x and the cosine function is replaced by the sine. The inverted algebraic system of equations for the unknown coefficients in (20) are recapitulated in Appendix A.

Choosing the Green function satisfying the Neumann condition on $z = 0$, the scattering potentials in the semi-infinite domain, $z \geq 0$, can be expressed as

$$\begin{aligned}
&\Psi_{M,sc}^{(0,1)}(s,\phi,\theta) \\
&= -\frac{1}{2\pi}\int_0^{2\pi}\int_0^1 \frac{\partial \Psi_{M,sc}^{(0,1)}}{\partial z}\Big|^{<} \frac{\rho_0\, d\rho_0 d\theta_0}{\sqrt{s^2+\rho_0^2-2\rho_0 s\sin\theta\cos(\phi-\phi_0)}},
\end{aligned} \tag{21}$$

where (s,ϕ,θ) is the spherical position coordinates, defined in Fig. 1. The integral will be integrated numerically for the demonstration purpose, c.f. Fig. 3. While moving away from the pore, $s \to \infty$,

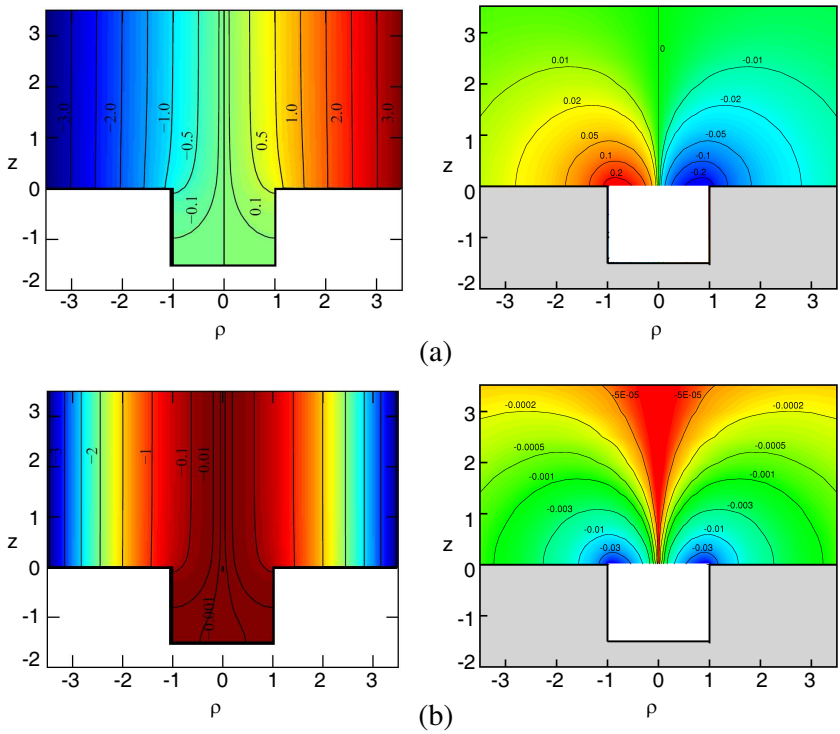

Figure 3. Magnetic scalar potentials of the inner field for $\ell = 1.5$ for (a) $O(1)$, on $\phi = \pi/2$ plane and (b) $O(\epsilon)$, on $\phi = \pi/4$ plane. The left column is the total field. The right column is the scattering multipoles, $\Psi^{(0,1)}_{M,sc}$, after substracting the external and the pore fields. They are (a) the dipole (1,1), and (b) the quadrupole $(2, 2)$. The fields are normalized by the incidence factors, which are 1 and ik_x, respectively.

the scattering potentials transit to the outer wave propagation region, with the characteristic length scale becoming the wavelength.

In order to match with the outer wave propagation field, we need to find the far field behaviors of (21). This is done by letting $s^2 = \rho^2 + z^2 \to \infty$ and expanding the denominator in the integrand by Taylor series with the small parameter ρ_0/s. After this expansion, the integrals can be integrated, for similar details see from (25) to (30)

in [17], and the approximations are found:

$$\Psi^{(0)}_{M,sc}(s,\phi,\theta) \approx -\frac{1}{2s^2}\bar{A}^{(0)}_{M,1n}\tanh(j'_{1n}\ell)J_2(j'_{1n})\sin\theta\sin\phi$$
$$+\frac{3}{16s^4}\bar{A}^{(0)}_{M,1n}\tanh(j'_{1n}\ell)\left(J_2(j'_{1n})-\frac{2}{j'_{1n}}J_3(j'_{1n})\right)\left(5\cos^2\theta-1\right)\sin\theta\sin\phi, \quad (22)$$

and

$$\Psi^{(1)}_{M,sc}(s,\phi,\theta) \approx -\frac{3ik_x}{8s^3}\bar{A}^{(1)}_{M,2n}\tanh(j'_{2n}\ell)J_3(j'_{2n})\sin^2\theta\sin(2\phi), \quad (23)$$

with an accuracy up to $O(s^{-4})$. The spatial dependence indicates that there are two near field singularities, s^{-2} and s^{-4}, of the scattering wave, and they become the wave radiation in the outer radiation field, which is described by the outgoing spherical Hankel function, $h^{(1)}_1(S)$ and $h^{(1)}_3(S)$, because of the matching singularity as $S \to 0$. Replacing the inner spatial variable s with the outer spatial variable $S = \epsilon s$ and substituting the spherical Hankel wave functions, the multipole radiation is obtained in the form of

$$\Psi_{M,sc}(S,\phi,\theta) = \epsilon^2\Psi^{(2)}_{M^{11},sc} + \epsilon^4\left(\Psi^{(4)}_{M^{31},sc} + \Psi^{(4)}_{M^{22},sc}\right) + \epsilon^4\tilde{\Psi}^{(4)}_{M,sc} \quad (24)$$

where the subscripts, $_{M^{11}}$, $_{M^{31}}$ and $_{M^{22}}$ are associated with the magnetic scalar potential and denote the scattering multipole modes. The multipoles of (24) are explicitly

$$\begin{aligned}
\Psi^{(2)}_{M^{11},sc} &= -\frac{i}{2}\bar{A}^{(0)}_{M,1n}\tanh(j'_{1n}\ell)J_2(j'_{1n})h^{(1)}_1(S)\sin\theta\sin\phi,\\
\Psi^{(4)}_{M^{31},sc} &= \frac{i}{80}\bar{A}^{(0)}_{M,1n}\tanh(j'_{1n}\ell)\left(J_2(j'_{1n}) - \frac{2}{j'_{1n}}J_3(j'_{1n})\right)\\
&\qquad h^{(1)}_3(S)\sin\theta(5\cos^2\theta-1)\sin\phi\\
\Psi^{(4)}_{M^{22},sc} &= \frac{k_x}{8}\bar{A}^{(1)}_{M,2n}\tanh(j'_{2n}\ell)J_3(j'_{2n})h^{(1)}_2(S)\sin^2\theta\sin(2\phi).
\end{aligned} \quad (25)$$

These modes are numbered on a similar scheme as in the quantum mechanics.There is an additional correction term arising from the higher order inner region to satisfy the gauge condition. The correction term, $\tilde{\Psi}^{(4)}_{M,sc}$, is of $O(\epsilon^4)$, c.f. (41). This structure of the higher order correction is also found in [11], except that we find it using the gauge condition. In our present notation, we keep the directivity patterns in the primitive triangular function forms instead of the spherical harmonics for convenience of calculation.

Having solved the magnetic potentials, we now work on the electric potentials, $\Psi^{(0,1)}_E$. The perfect conducting boundary condition that

these electric potentials satisfy is the Dirichlet condition $\Psi_E^{(0,1)} = 0$. This corresponds to the acoustic scattering with a pressure-release (soft) condition so that we can derive the integral equations for the scattering components $\Psi_{E,sc}^{(0,1)}$, see Section 4 in [17],

$$\int_0^{2\pi}\int_0^1 \frac{\partial \Psi_{E,sc}^{(0,1)}}{\partial z_0}\Big|^{<} \frac{\rho_0 d\rho_0 d\phi_0}{\sqrt{\rho^2+\rho_0^2-2\rho_0\rho\cos(\phi-\phi_0)}} = -\int_0^{2\pi}\int_1^{\infty} \frac{\partial \Psi_{E,sc}^{(0,1)}}{\partial z_0}\Big|^{>} \frac{\rho_0 d\rho_0 d\phi_0}{\sqrt{\rho^2+\rho_0^2-2\rho_0\rho\cos(\phi-\phi_0)}}, \quad (26)$$

where the evaluation symbol, $|^{>}$, represents that its operand is evaluated on the areas $\rho \geq 1$, $z = 0$. Similar to the magnetic counterpart, the electric potentials satisfying (26), the resultant potentials in the semi-infinite domain $z \geq 0$ and in the pore $0 \leq \rho 1$, $z < 0$ are, respectively,

$$\Psi_E^{(0,1)} = \Psi_{E,ext}^{(0,1)} + \Psi_{E,sc}^{(0,1)}, \qquad \Psi_E^{(0,1)} = \Psi_{E,pore}^{(0,1)}, \quad (27)$$

and they are smoothly continuous across the pore exit plane. The external forcing electric potentials, defined in the first and third terms in (16), are $\Psi_{E,ext}^{(0)} = -k_x z$ and $\Psi_{E,ext}^{(1)} = -ik_x^2 \rho z \cos\phi$, (16) and the potentials in the pore can be expanded by the eigen-solutions

$$\begin{aligned}
\Psi_{E,pore}^{(0)}(\rho,\phi,z) &= -k_x \frac{\bar{A}_{E,0n}^{(0)}}{j_{0n}} J_0(j_{0n}\rho)\frac{\sinh(j_{0n}(z+\ell))}{\cosh(j_{0n}\ell)},\\
\Psi_{E,pore}^{(1)}(\rho,\phi,z) &= -ik_x^2 \frac{\bar{A}_{E,1n}^{(1)}}{j_{1n}} J_1(j_{1n}\rho)\cos\phi\frac{\sinh(j_{1n}(z+\ell))}{\cosh(j_{1n}\ell)},
\end{aligned} \quad (28)$$

where j_{mn} satisfies $J_m(j_{mn}) = 0$. The coefficients in (28) with (26) can be analytically inverted and the results are relegated to Appendix A. The equations and their solutions are analogous to those of the acoustic scattering with the pressure-release boundaries, see (42) in [17], provided that the acoustic incident wave ik_z and $k_x k_z$ are replaced by k_x and $-ik_x^2$.

The scattering field in $z \geq 0$ can be found with the help of the Green function that vanishes on $z = 0$

$$\Psi_{E,sc}^{(0,1)}(s,\phi,\theta) = \frac{1}{2\pi}\int_0^{2\pi}\int_0^1 \Psi_{E,sc}^{(0,1)}|^{<} \frac{s\cos\theta}{(s^2+\rho_0^2-2\rho_0 s\sin\theta\cos(\phi-\phi_0))^{3/2}}\rho_0 d\rho_0 d\phi_0, \quad (29)$$

where we use the spherical coordinates for the semi-infinite domain. Numerical example of the above expression will be given in c.f. Fig. 5.

To resolve into the wave radiation multipoles, we first approximate the far-field of the above scatter field by letting $s^2 = \rho^2 + z^2 \to \infty$. After Taylor expansion against ρ_0/s, substitution of (28) and integration, the only non-vanishing terms of the integrals are

$$\Psi^{(0)}_{E,sc}(s,\phi,\theta) \approx -\frac{k_x}{s^2}\frac{\bar{A}^{(0)}_{E,0n}}{j^2_{0n}}\tanh(j_{0n}\ell)J_1(j_{0n})\cos\theta$$
$$+\frac{3k_x}{2s^4}\frac{\bar{A}^{(0)}_{E,0n}}{j^2_{0n}}\tanh(j_{0n}\ell)\left(J_1(j_{0n})-\frac{2}{j_{0n}}J_2(j_{0n})\right)\left(\frac{5}{2}\cos^2\theta-\frac{3}{2}\right)\cos\theta, \quad (30)$$

and

$$\Psi^{(1)}_{E,sc}(s,\phi,\theta) \approx -\frac{3ik_x^2}{2s^3}\frac{\bar{A}^{(1)}_{E,1n}}{j^2_{1n}}\tanh(j_{1n}\ell)J_2(j_{1n})\sin\theta\cos\theta\cos\phi, \quad (31)$$

with the same accuracy $O(s^{-4})$ as for the magnetic scalar potentials. Recasting the inner spatial radial coordinate s with the outer $S = \epsilon s$ and with the spatial singularities and the directivity patterns, we match the radiation multipoles to be

$$\Psi_{E,sc}(S,\phi,\theta) = \epsilon^2\Psi^{(2)}_{E^{10},sc} + \epsilon^4\left(\Psi^{(4)}_{E^{30},sc} + \Psi^{(4)}_{E^{21},sc}\right) + \epsilon^4\tilde{\Psi}^{(4)}_{E,sc} \quad (32)$$

whereas

$$\begin{aligned}
\Psi^{(2)}_{E^{10},sc} &= -\frac{ik_x\bar{A}^{(0)}_{E,0n}}{j^2_{0n}}\tanh(j_{0n}\ell)J_1(j_{0n})h^{(1)}_1(S)\cos\theta,\\
\Psi^{(4)}_{E^{30},sc} &= \frac{ik_x}{20}\frac{\bar{A}^{(0)}_{E,0n}}{j^2_{0n}}\tanh(j_{0n}\ell)\left(J_1(j_{0n}) - \frac{2}{j_{0n}}J_2(j_{0n})\right)\\
&\quad h^{(1)}_3(S)\cos\theta(5\cos^2\theta - 3)\\
\Psi^{(4)}_{E^{21},sc} &= \frac{k_x^2}{2}\frac{\bar{A}^{(1)}_{E,1n}}{j^2_{1n}}\tanh(j_{1n}\ell)J_2(j_{1n})h^{(1)}_2(S)\sin\theta\cos\theta\cos\phi.
\end{aligned} \quad (33)$$

Similar to the magnetic potential (24), the radiation (32) is completed by including a correction term, $\tilde{\Psi}^{(4)}_{E,sc}$, from the higher order inner field, c.f. (44), to satisfy the gauge condition.

Equations (25) and (33) are the radiation fields induced by the leading orders, $O(\epsilon^0)$ and $O(\epsilon)$, of the electric and magnetic inner potentials. The characteristics of the inner static potentials are reported in Garcia de Abajo and Saenz [2], using numerical investigations into the near field of the electromagnetic waves near rectangular pores. These radiation potentials, however, are not able to completely describe the outer radiation electro/magneto-fields

because the conjugate vector potentials have to be taken into account. Although these conjugate potentials are induced by the scalar ones and appear in the higher order of the inner region, they can radiate lower orders of multipoles which balance with the scalar potentials, c.f. the first terms of (36) and (43), according to (10). They will be described in the following two sections.

3.3. Electric Vector Potential and Associated Higher Order Corrections

With the solved magnetic scalar potentials $\Psi_M^{(0,1)}$, we now use the gauge condition $(11)_3$ to solve for the their conjugate electric vector potentials in the inner region. These vector potentials in general have the cylindrical coordinate components

$$\mathbf{A}_E^{(1,2)}(\rho,\phi,z) = \mathbf{e}_\rho \mathrm{A}_{E_\rho}^{(1,2)} + \mathbf{e}_\phi \mathrm{A}_{E_\phi}^{(1,2)} + \mathbf{e}_z \mathrm{A}_{E_z}^{(1,2)}. \tag{34}$$

The complexity of the solving procedures is greatly simplified if we first inspect the potential in the pore region. With the magnetic potentials in the pore (20), we can express the components of the vector potentials of the two orders, respectively, in the form of

$$\begin{aligned}
\mathrm{A}_{E_\rho,pore}^{(1)} =& D_n^{(1)} J_0(j'_{1n}\rho)\sin\phi \frac{\cosh(j'_{1n}(z+\ell))}{\cosh(j'_{1n}\ell)} \\
&+ F_n^{(1)} J_2(j'_{1n}\rho)\sin\phi \frac{\cosh(j'_{1n}(z+\ell))}{\cosh(j'_{1n}\ell)}, \\
\mathrm{A}_{E_\phi,pore}^{(1)} =& D_n^{(1)} J_0(j'_{1n}\rho)\cos\phi \frac{\cosh(j'_{1n}(z+\ell))}{\cosh(j'_{1n}\ell)} \\
&- F_n^{(1)} J_2(j'_{1n}\rho)\cos\phi \frac{\cosh(j'_{1n}(z+\ell))}{\cosh(j'_{1n}\ell)}, \\
\mathrm{A}_{E_z,pore}^{(1)} =& E_n^{(1)} J_1(j'_{1n}\rho)\sin\phi \frac{\sinh(j'_{1n}(z+\ell))}{\cosh(j'_{1n}\ell)},
\end{aligned} \tag{35}$$

and

$$\begin{aligned}
\mathrm{A}_{E_\rho,pore}^{(2)} =& D_n^{(2)} J_1(j'_{2n}\rho)\sin(2\phi) \frac{\cosh(j'_{2n}(z+\ell))}{\cosh(j'_{2n}\ell)} \\
&+ F_n^{(2)} J_3(j'_{2n}\rho)\sin(2\phi) \frac{\cosh(j'_{2n}(z+\ell))}{\cosh(j'_{2n}\ell)}, \\
\mathrm{A}_{E_\phi,pore}^{(2)} =& D_n^{(2)} J_1(j'_{2n}\rho)\cos(2\phi) \frac{\cosh(j'_{2n}(z+\ell))}{\cosh(j'_{2n}\ell)} \\
&- F_n^{(2)} J_3(j'_{2n}\rho)\cos(2\phi) \frac{\cosh(j'_{2n}(z+\ell))}{\cosh(j'_{2n}\ell)},
\end{aligned}$$

$$\mathrm{A}^{(2)}_{E_z,pore} = E_n^{(2)} J_2(j'_{2n}\rho)\sin(2\phi)\frac{\sinh(j'_{2n}(z+\ell))}{\cosh(j'_{2n}\ell)}.$$

Substituting into $(11)_3$, we have the equations for the unknown coefficients

$$D_n^{(1)} - E_n^{(1)} - F_n^{(1)} = \frac{i\bar{A}^{(0)}_{M,1n}}{j'_{1n}}, \quad D_n^{(2)} - E_n^{(2)} - F_n^{(2)} = -\frac{k_x \bar{A}^{(1)}_{M,2n}}{j'_{2n}},$$

These particular azimuthal dependencies of the vector potentials are directly associated with the inducing scalar potentials. For general azimuthal modes, one can apply the method described in [20].

Without needing to go into the rigorous procedures as in [20], the above vector potentials can be illustrated to satisfy the Laplace equation in the inner regions by recasting them into the Cartesian component form. Taking (35) as the example; its Cartesian components read

$$\begin{aligned}\mathbf{A}^{(1)}_{E,pore} = {} & D_n^{(1)} \begin{pmatrix} 0 \\ 1 \\ 0 \end{pmatrix} J_0(j'_{1n}\rho)\frac{\cosh(j'_{1n}(z+\ell))}{\cosh(j'_{1n}\ell)} \\ & + F_n^{(1)} \begin{pmatrix} \sin(2\phi) \\ -\cos(2\phi) \\ 0 \end{pmatrix} J_2(j'_{1n}\rho)\frac{\cosh(j'_{1n}(z+\ell))}{\cosh(j'_{1n}\ell)} \\ & + E_n^{(1)} \begin{pmatrix} 0 \\ 0 \\ \sin\phi \end{pmatrix} J_1(j'_{1n}\rho)\frac{\sinh(j'_{1n}(z+\ell))}{\cosh(j'_{1n}\ell)}.\end{aligned}$$

They obviously satisfy the Laplace equation component-wisely. From the perfect conducting boundary condition of the electric field, we have that the x- and y-components are of the Neumann type and the z-component is of the Dirichlet type on the flanged and the bottom surfaces of the pore. The scattering field in the semi-infinite domain, $z \geq 0$, therefore, can be found using the correspondent integral representations, e.g., similar to (21) and (29), for the two boundary types, respectively. After matching to the outer region by following the similar process for the scalar potential radiation, we find the leading two orders, $O(\epsilon^2)$ and $O(\epsilon^4)$, of the radiation vector potential fields

$$\begin{aligned}\hat{\mathbf{A}}_{E,sc} = {} & -i\epsilon^2 D_n^{(1)} \tanh(j'_{1n}\ell) J_1(j'_{1n}) \begin{pmatrix} 0 \\ 1 \\ 0 \end{pmatrix} h_0^{(1)}(S) \\ & + \epsilon^4 \frac{iE_n^{(1)}}{2j'_{1n}} J_2(j'_{1n}) \tanh(j'_{1n}\ell) \begin{pmatrix} 0 \\ 0 \\ \sin\phi \end{pmatrix} h_2^{(1)}(S)\sin\theta\cos\theta\end{aligned}$$

$$-\epsilon^4\frac{i}{12}D_n^{(1)}\tanh(j'_{1n}\ell)\left(J_1(j'_{1n})-\frac{2}{j'_{1n}}J_2(j'_{1n})\right)\begin{pmatrix}0\\1\\0\end{pmatrix}h_2^{(1)}(S)\left(1-3\cos^2\theta\right)$$

$$-\epsilon^4\frac{i}{8}F_n^{(1)}J_3\left(j'_{1n}\right)\tanh(j'_{1n}\ell)\begin{pmatrix}\sin(2\phi)\\-\cos(2\phi)\\0\end{pmatrix}h_2^{(1)}(S)\sin^2\theta. \quad (36)$$

Similarly, the radiation to $O(\epsilon^4)$ from the second order inner vector potential field, $\mathbf{A}_E^{(2)}$, is

$$\tilde{\mathbf{A}}_{E,sc}=-\epsilon^4\frac{iD_n^{(2)}}{2}J_2(j'_{2n})\tanh(j'_{2n}\ell)\begin{pmatrix}\sin\phi\\\cos\phi\\0\end{pmatrix}h_1^{(1)}(S)\sin\theta. \quad (37)$$

Sorting these radiation terms, we obtain the resultant radiation field to be

$$\begin{aligned}\mathbf{A}_{E,sc}&=\hat{\mathbf{A}}_{E,sc}+\tilde{\mathbf{A}}_{E,sc}\\&=\epsilon^2\begin{pmatrix}0\\\mathrm{A}^{(2)}_{E_y^{00},sc}\\0\end{pmatrix}+\epsilon^4\begin{pmatrix}\mathrm{A}^{(4)}_{E_x^{22},sc}+\mathrm{A}^{(4)}_{E_x^{11},sc}\\\mathrm{A}^{(4)}_{E_y^{20},sc}+\mathrm{A}^{(4)}_{E_y^{22},sc}+\mathrm{A}^{(4)}_{E_y^{11},sc}\\\mathrm{A}^{(4)}_{E_y^{21},sc}\end{pmatrix}, \quad (38)\end{aligned}$$

to the accuracy of $O(\epsilon^4)$ in the outer region. The suffices like E_y^{00}, E_x^{22}, etc., are collected according to the multipole directivity of the potential components.

Now, we can solve the unknown coefficients using the outer gauge condition $(9)_3$. With the potential radiation (24), the coefficient $D_n^{(1)}$ can be solved

$$D_n^{(1)}=\frac{i\bar{A}^{(0)}_{M,1n}}{2j'_{1n}}, \quad (39)$$

from the gauge condition of $O(\epsilon^2)$ and the other coefficients

$$E_n^{(1)}=0,\qquad F_n^{(1)}=-\frac{i\bar{A}^{(0)}_{M,1n}}{2j'_{1n}},\qquad D_n^{(2)}=-\frac{k_x}{2}\frac{\bar{A}^{(1)}_{M,2n}}{j'_{2n}}, \quad (40)$$

from the gauge condition of $O(\epsilon^4)$. The higher order correction of the magnetic scalar potential radiation, see (24), is found to be a dipole

$$\begin{aligned}&\epsilon^4\tilde{\Psi}^{(4)}_{M,sc}=\epsilon^4\Psi^{(4)}_{M^{11},sc}\\&=-\epsilon^4\frac{i}{30}\frac{\bar{A}^{(0)}_{M,1n}}{j'_{1n}}\tanh(j'_{1n}\ell)\left(2J_3(j'_{1n})-\frac{1}{j'_{1n}}J_2(j'_{1n})\right)h_1^{(1)}(S)\sin\phi\sin\theta, \quad (41)\end{aligned}$$

which leads to $O(\epsilon^2)$ in the inner field. The scalar potential radiation (24) and the notation definitions of the vector components in (38) are summarized in Table 1.

Inspecting the radiation terms to $O(\epsilon^4)$ in Table 1, we find that they are solely determined by the two inner scalar potentials, $\Psi^{(0)}_{M,sc}$ and $\Psi^{(1)}_{M,sc}$. As an example, we solve numerically for the coefficients and construct the inner potential fields. For $\ell = 1.5$, the convergence properties of the inversed algebraic system, c.f. Appendix A, has been verified in Kuo et al. [17], that if the coefficients are truncated to $N = 120$ terms, we produce an relative error no more than approximately 3% at the singular pore exit corner. Figures 3(a) and (b) show the scattering potentials, (21), of $O(1)$ and $O(\epsilon)$ on the $\phi = \pi/2$ and $\pi/4$ cut planes. They are normalized by the incident angle factors 1 and

Table 1. Magnetic dipole radiation and its associated radiation of $O(\epsilon^4)$. The summation operator from $n = 1$ to ∞ is omitted. For TE incident, multiply each component of the scalar potentials with k_z and exchange $\sin\phi$ and $\sin(2\phi)$ by $\cos\phi$ and $\cos(2\phi)$, c.f. Section 4 Trivial adjustments of the conjugate vector potentials can be found straightforwardly using the gauge condition.

Scalar magnetic potential	Multipole moment coefficients
$\Psi^{(2)}_{M^{11},sc} = -i\bar{B}^{(2)}_{M^{11}} h^{(1)}_1(S)\sin\theta\sin\phi$	$\bar{B}^{(2)}_{M^{11}} = \frac{1}{2}\bar{A}^{(0)}_{M,1n}\tanh(j'_{1n}\ell)J_2(j'_{1n})$
$\Psi^{(4)}_{M^{31},sc} = i\bar{B}^{(4)}_{M^{31}} h^{(1)}_3(S)$	$\bar{B}^{(4)}_{M^{31}} = \frac{1}{80}\bar{A}^{(0)}_{M,1n}\tanh(j'_{1n}\ell)$
$\sin\theta(5\cos^2\theta - 1)\sin\phi$	$\left(J_2(j'_{1n}) - \frac{2}{j'_{1n}}J_3(j'_{1n})\right)$
$\Psi^{(4)}_{M^{22},sc} = k_x\bar{B}^{(4)}_{M^{22}} h^{(1)}_2(S)\sin^2\theta\sin(2\phi)$	$\bar{B}^{(4)}_{M^{22}} = \frac{1}{8}\bar{A}^{(1)}_{M,2n}\tanh(j'_{2n}\ell)J_3(j'_{2n})$
$\Psi^{(4)}_{M^{11},sc} = -i\bar{B}^{(4)}_{M^{11}} h^{(1)}_1(S)\sin\phi\sin\theta$	$\bar{B}^{(4)}_{M^{11}} = \frac{1}{30}\frac{\bar{A}^{(0)}_{M,1n}}{j'_{1n}}\tanh(j'_{1n}\ell)$
	$\left(2J_3(j'_{1n}) - \frac{1}{j'_{1n}}J_2(j'_{1n})\right)$
Vector electric potential	**Multipole moment coefficients**
$\mathrm{A}^{(2)}_{E^{00}_y,sc} = \bar{C}^{(2)}_{E^{00}} h^{(1)}_0(S)$	$\bar{C}^{(2)}_{E^{00}} = \frac{\bar{A}^{(0)}_{M,1n}}{2j'_{1n}}J_1(j'_{1n})\tanh(j'_{1n}\ell) = \bar{B}^{(2)}_{M^{11}}$
$\mathrm{A}^{(4)}_{E^{22}_x,sc} = -\bar{C}^{(4)}_{E^{22}} h^{(1)}_2(S)\sin^2\theta\sin(2\phi)$	$\bar{C}^{(4)}_{E^{22}} = \frac{\bar{A}^{(0)}_{M,1n}}{16j'_{1n}}J_3(j'_{1n})\tanh(j'_{1n}\ell)$
$\mathrm{A}^{(4)}_{E^{11}_x,sc} = ik_x\bar{C}^{(4)}_{E^{11}} h^{(1)}_1(S)\sin\theta\sin\phi$	$\bar{C}^{(4)}_{E^{11}} = \frac{\bar{A}^{(1)}_{M,2n}}{4j'_{2n}}J_2(j'_{2n})\tanh(j'_{2n}\ell)$
$\mathrm{A}^{(4)}_{E^{20}_y,sc} = -\bar{C}^{(4)}_{E^{20}} h^{(1)}_2(S)(3\cos^2\theta - 1)$	$\bar{C}^{(4)}_{E^{20}} = \frac{\bar{A}^{(0)}_{M,1n}}{24j'_{1n}}\tanh(j'_{1n}\ell)$
	$\left(J_1(j'_{1n}) - \frac{2}{j'_{1n}}J_2(j'_{1n})\right)$
$\mathrm{A}^{(4)}_{E^{22}_y,sc} = \bar{C}^{(4)}_{E^{22}} h^{(1)}_2(S)\sin^2\theta\cos(2\phi)$	
$\mathrm{A}^{(4)}_{E^{11}_y,sc} = ik_x\bar{C}^{(4)}_{E^{11}} h^{(1)}_1(S)\sin\theta\cos\phi$	

ik_x, respectively. Our focus is drawn to the lobe structures, the leading term of (22) and (23), of the multipole inner scattering fields, the right pannels in Fig. 3. They are respectively a dipole in the y-direction and a quadrupole of $(2, 2)$. The multipole moment coefficients, the strengths of the radiation terms, $\bar{B}^{(2,4)}_{M^{mn}}$ and $\bar{C}^{(2,4)}_{E^{mn}}$, are the functions of the pore depth ℓ, as depicted in Fig. 4. They all increase from zero as ℓ increases from zero, and saturate to their constant values when ℓ is larger than about 1.

Another striking feature is that the multipoles are not organized in a strictly ascending manner but exhibit an intervened structure. For example, in $O(\epsilon^4)$ of the radiation field, the scattering scalar potential wave is composed of an octupole, a quadrupole, and a dipole, and the Cartesian components of the electric vector potential consist of quadrupoles and dipoles. This is due to the finite size effect of the pore.

Up to this point, we have only used the gauge condition to determine the unknown coefficients for the radiation. We need to verify if the solution satisfies the boundary condition in the pore. The electric

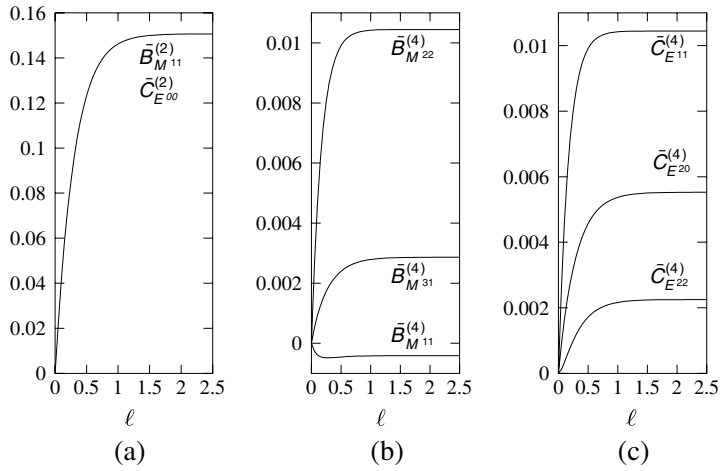

Figure 4. Multipole moment coefficients versus the pore depth, associated with the electric potentials. (a) coefficients for $O(\epsilon^2)$, (b) coefficients for $O(\epsilon^4)$ electric scalar potentials, (c) coefficients for $O(\epsilon^4)$ magnetic vector potentials.

field reads

$$\mathbf{E}^{(1)}_{pore} = -\nabla_i \times \mathrm{A}^{(1)}_{E,pore}$$
$$= -\frac{i\bar{A}^{(0)}_{M,1n}}{j'_{1n}} \frac{\sinh(j'_{1n}(z+\ell))}{\rho\cosh(j'_{1n}\ell)} \left(\mathbf{e}_\rho J_1(j'_{1n}\rho)\cos\phi + \mathbf{e}_\phi j'_{1n} J'_1(j'_{1n}\rho)\sin\phi\right).$$

It is clear that the field fulfills the vanishing tangential electric field on the perfect conducting surface in the pore. The zero z-component in the pore indicates that the conjugate electric field with the magnetic scalar potential is a transverse electric (TE) waveguide mode.

The leading order radiation of the magnetic and electric fields, associated with the magnetic potential, $\Psi^{(2)}_{M^{11},sc}$, and the electric vector potential, $\mathrm{A}^{(2)}_{E^{00}_y,sc}$, are obtained by using the definition of the electric vector potential and $(10)_1$, and they are explicitly

$$\begin{aligned}
\mathbf{E}^{(3)}_{TE} &= \epsilon^3 \frac{e^{iS}}{S} \bar{B}^{(2)}_{M^{11}} \begin{pmatrix} 0, \\ \cos\phi, \\ -\cos\theta\sin\phi \end{pmatrix}_{\text{spherical}}, \\
\mathbf{B}^{(3)}_{TE} &= \epsilon^3 \frac{e^{iS}}{S} \bar{B}^{(2)}_{M^{11}} \begin{pmatrix} 0, \\ \cos\theta\sin\phi, \\ \cos\phi \end{pmatrix}_{\text{spherical}},
\end{aligned} \tag{42}$$

in the spherical coordinate. We have also omitted terms smaller than $O(S^{-2})$ for clarity. Unlike the field radiation of a electro-magnetic dipole, (42) is a dipole aligning in the $\mathbf{e}_y$ direction at the pore exit, and its strength does not depend on the incident angle. The $_{TE}$ suffix of the fields are given because the fields in the pore correspond to a TE waveguide mode.

3.4. Magnetic Vector Potential and Associated Higher Order Corrections

The magnetic vector potential and its higher order corrections can be found in the same way as the electric vector potential in the previous section. Without repeating the details, we only represent the calculation results.

The two leader orders of the inner magnetic vector potentials are found in a much simpler form than their electric counterparts, which contain only the z-components

$$\mathbf{A}^{(1)}_{M,pore} = \mathbf{e}_z i k_x \frac{\bar{A}^{(0)}_{E,0n}}{j^2_{0n}} J_0(j_{0n}\rho) \frac{\cosh(j_{0n}(z+\ell))}{\cosh(j_{0n}\ell)},$$

$$\mathbf{A}^{(2)}_{M,pore} = -\mathbf{e}_z k_x^2 \frac{\bar{A}^{(1)}_{E,1n}}{j_{1n}^2} J_1(j_{1n}\rho)\cos\phi \frac{\cosh(j_{1n}(z+\ell))}{\cosh(j_{1n}\ell)}.$$

The magnetic fields associated with the two orders of the magnetic vector potentials are

$$\mathbf{B}^{(1)}_{pore} = \nabla_i \times \mathbf{A}^{(1)}_{M,pore} = \mathbf{e}_\phi \frac{ik_x}{j_{0n}} \bar{A}^{(0)}_{E,0n} \frac{\cosh(j_{0n}(z+\ell))}{\rho\cosh(j_{0n}\ell)} J_1(j_{0n}\rho),$$

$$\mathbf{B}^{(2)}_{pore} = \nabla_i \times \mathbf{A}^{(2)}_{M,pore} = k_x^2 \frac{\bar{A}^{(1)}_{E,1n}}{2j_{1n}} \frac{\cosh(j_{1n}(z+\ell))}{\cosh(j_{1n}\ell)}$$
$$\Big(\mathbf{e}_\rho(J_0(j_{1n}\rho)+J_2(j_{1n}\rho))\sin\phi + \mathbf{e}_\phi(J_0(j_{1n}\rho)-J_2(j_{1n}\rho))\cos\phi\Big),$$

which obviously correspond to TM waveguide modes.

With the perfect conducting surface condition, the z-component of the magnetic vector potential satisfies the Neumann condition on the flanged surface. The radiation of the vector potential can be found using an integral relation similar to (21), which leads to

$$\begin{aligned}
\mathbf{A}_{M,sc} &= \epsilon^2 \mathbf{e}_z k_x \frac{\bar{A}^{(0)}_{E,0n}}{j_{0n}^2} \tanh(j_{0n}\ell) J_1(j_{0n}) h_0^{(1)}(S) \\
&+\epsilon^4 \mathbf{e}_z \frac{k_x}{12} \frac{\bar{A}^{(0)}_{E,0n}}{j_{0n}^2} \tanh(j_{0n}\ell)\left(J_1(j_{0n}) - \frac{2}{j_{0n}} J_2(j_{0n})\right) h_2^{(1)}(S)\left(1-3\cos^2\theta\right) \\
&+\epsilon^4 \mathbf{e}_z \frac{ik_x^2}{2} \frac{\bar{A}^{(1)}_{E,1n}}{j_{1n}^2} J_2(j_{1n}) \tanh(j_{1n}\ell) h_1^{(1)}(S) \sin\theta\cos\phi \\
&= \epsilon^2 \mathbf{e}_z \mathrm{A}^{(2)}_{M_z^{00},sc} + \epsilon^4 \mathbf{e}_z \mathrm{A}^{(4)}_{M_z^{20},sc} + \epsilon^4 \mathbf{e}_z \mathrm{A}^{(4)}_{M_z^{11},sc}.
\end{aligned} \tag{43}$$

The higher order correction of the electric scalar potential to the radiation, the last term of (32), is obtained by employing the gauge condition $(9)_3$

$$\begin{aligned}
\tilde{\Psi}^{(4)}_{E,sc} &= \Psi^{(4)}_{E^{10},sc} \\
&= -\frac{ik_x}{15} \frac{\bar{A}^{(0)}_{E,0n}}{j_{0n}^2} \tanh(j_{0n}\ell)\left(J_1(j_{0n}) - \frac{2}{j_{0n}} J_2(j_{0n})\right) h_1^{(1)}(S)\cos\theta.
\end{aligned} \tag{44}$$

These radiation components up to $O(\epsilon^4)$ are summarized in Table 2.

We take the same case, $\ell = 1.5$ for numerical demonstration of the inner scalar electric potential fields. Figs. 5(a), (b) show the inner potentials, (28) and (29), $\Psi^{(0)}_{E,sc}$ and $\Psi^{(1)}_{E,sc}$ normalized by $-k_x$ and

$-ik_x^2$. From their lobe structure and directivities in $z \geq 0$, the first term of (30) and (31), the former is a vertical dipole and the latter is a quadrupole $(2,1)$. Varying ℓ, we obtain the multipole moment coefficients as functions of the pore depth, Fig. 6. They show the common characteristics of the previous magnetic scalar potentials, that they are zero at $\ell = 0$ and saturate to their respective constant values when ℓ is larger than about 1. In addition, the multipoles all vanish when the incident wave is normally shed on the pore because they depend on the incident factors k_x and k_x^2.

The leading electric and magnetic radiation fields are obtained using $(10)_2$ with the potentials $\Psi^{(0)}_{E^{10},sc}$ and $\mathrm{A}^{(1)}_{M_z^{00},sc}$, and they are

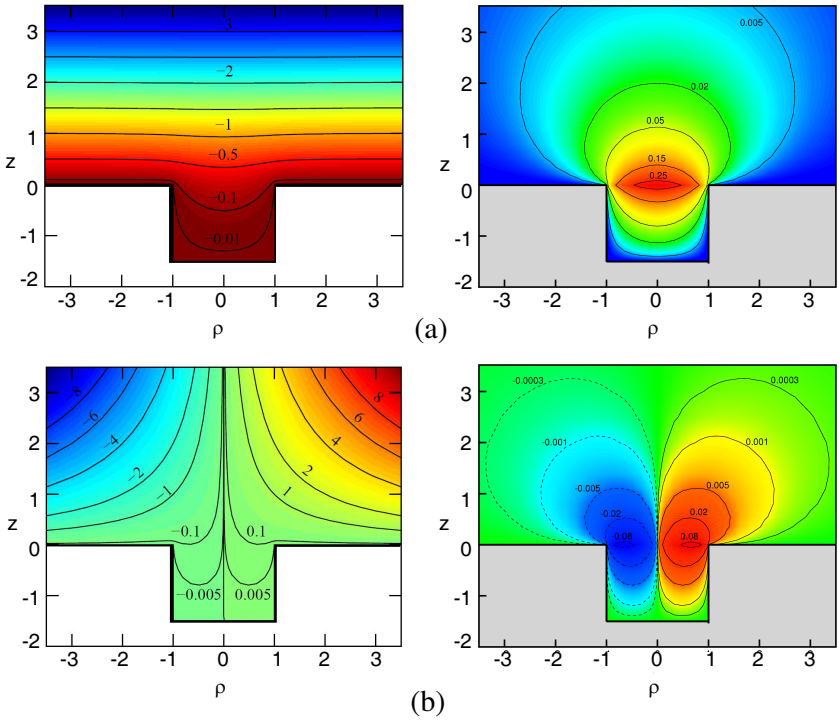

Figure 5. Electric scalar potentials of the inner field for $\ell = 1.5$ for (a) $O(1)$ plane and (b) $O(\epsilon)$, on $\phi = 0$ plane. The left column is the total field. The right column is the scattering multipoles, $\Psi^{(0,1)}_{E,sc}$, after subtracting the external forcing field. They are (a) the dipole (1,0), and (b) the quadrupole $(2,1)$. The fields are normalized by the incidence factors, which are $-k_x$ and $-ik_x^2$, respectively.

Table 2. Electric dipole radiation and its associated radiation of $O(\epsilon^4)$. The summation operator from $n = 1$ to ∞ is omitted.

Scalar electric potential	Multipole moment coefficients
$\Psi^{(2)}_{E^{10},sc} = -ik_x \bar{B}^{(2)}_{E^{10}} h^{(1)}_1(S)\cos\theta$	$\bar{B}^{(2)}_{E^{10}} = \frac{\bar{A}^{(0)}_{E,0n}}{j^2_{0n}} \tanh(j_{0n}\ell) J_1(j_{0n})$
$\Psi^{(4)}_{E^{30},sc} = ik_x \bar{B}^{(4)}_{E^{30}} h^{(1)}_3(S)\cos\theta(5\cos^2\theta - 3)$	$\bar{B}^{(4)}_{E^{30}} = \frac{1}{20} \frac{\bar{A}^{(0)}_{E,0n}}{j^2_{0n}} \tanh(j_{0n}\ell) \left(J_1(j_{0n}) - \frac{2}{j_{0n}} J_2(j_{0n})\right)$
$\Psi^{(4)}_{E^{21},sc} = k^2_x \bar{B}^{(4)}_{E^{21}} h^{(1)}_2(S)\sin\theta\cos\theta\cos\phi$	$\bar{B}^{(4)}_{E^{21}} = \frac{1}{2} \frac{\bar{A}^{(1)}_{E,1n}}{j^2_{1n}} \tanh(j_{1n}\ell) J_2(j_{1n})$
$\Psi^{(4)}_{E^{10},sc} = -ik_x \bar{B}^{(4)}_{E^{10}} h^{(1)}_1(S)\cos\theta$	$\bar{B}^{(4)}_{E^{10}} = \frac{1}{15} \frac{\bar{A}^{(0)}_{E,0n}}{j^2_{0n}} \tanh(j_{0n}\ell) \left(J_1(j_{0n}) - \frac{2}{j_{0n}} J_2(j_{0n})\right)$
Vector magnetic potential	**Multipole moment coefficients**
$\mathrm{A}^{(2)}_{M^{00}_z,sc} = k_x \bar{C}^{(2)}_{M^{00}} h^{(1)}_0(S)$	$\bar{C}^{(2)}_{M^{00}} = \bar{B}^{(2)}_{E^{10}}$
$\mathrm{A}^{(4)}_{M^{20}_z,sc} = -k_x \bar{C}^{(4)}_{M^{20}} h^{(1)}_2(S)(3\cos^2\theta - 1)$	$\bar{C}^{(4)}_{M^{20}} = \frac{\bar{A}^{(0)}_{E,0n}}{12 j^2_{0n}} \tanh(j_{0n}\ell) \left(J_1(j_{0n}) - \frac{2}{j_{0n}} J_2(j_{0n})\right)$
$\mathrm{A}^{(4)}_{M^{11}_z,sc} = ik^2_x \bar{C}^{(4)}_{M^{11}} h^{(1)}_1(S)\sin\theta\cos\phi$	$\bar{C}^{(4)}_{M^{11}} = \frac{\bar{A}^{(1)}_{E,1n}}{2 j^2_{1n}} J_2(j_{1n}) \tanh(j_{1n}\ell)$

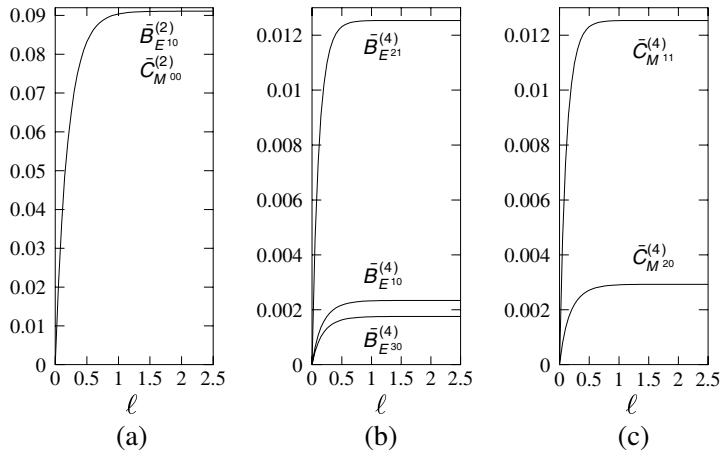

Figure 6. Multipole moment coefficients versus the pore depth, associated with the electric potentials. (a) coefficients for $O(\epsilon^2)$, (b) coefficients for $O(\epsilon^4)$ electric scalar potentials, (c) coefficients for $O(\epsilon^4)$ magnetic vector potentials.

explicitly

$$\begin{aligned}\mathbf{E}_{TM}^{(3)} &= -\epsilon^3 k_x \bar{B}_{E^{10}}^{(2)} \frac{e^i S}{S} \sin\theta \mathbf{e}_\theta, \\ \mathbf{B}_{TM}^{(3)} &= -\epsilon^3 k_x \bar{B}_{E^{10}}^{(2)} \frac{e^i S}{S} \sin\theta \mathbf{e}_\phi,\end{aligned} \tag{45}$$

in the spherical coordinate. This is the resultant field of a dipole aligning in the $\mathbf{e}_z$ direction at the pore exit. The $_{TM}$ suffix indicates that the fields are associated with a TM wave guidemode in the pore. The vertical dipole strength is $-k_x \bar{B}_{E^{10}}^{(2)}$ and, because it is proportional to k_x, excitation of this mode depends on the nonzero inclination angle. A physical intuition can be drawn that the nonzero incident angle introduces an external electrical forcing component in the z-direction, hence creating voltage potential differences in this direction and resulting in the vertical dipole radiation.

4. TRANSVERSE ELECTRIC POLARIZED INCIDENCE

We consider the TE polarized incidence in this section. The external wave field, the sum of the incident wave and its total reflective wave by the flanged perfect conducting surface, is

$$\mathbf{E}_{ext}^* = -2i|E_{inc}^*| \begin{pmatrix} 0 \\ 1 \\ 0 \end{pmatrix} \exp(ik_x^* x^*) \sin(k_z^* z^*).$$

From the Maxwell Equation (1), the external magnetic field is

$$i\omega^* \mathbf{B}^*{}_{ext} = -2i|E_{inc}^*| \begin{pmatrix} -k_z^* \cos(k_z^* z^*) \\ 0 \\ ik_x^* \sin(k_z^* z^*) \end{pmatrix} \exp(ik_x^* x^*).$$

After nondimensionalization and expansion in the inner region, the forcing, expressed by the potentials, becomes

$$\mathbf{E}_{ext} = i\epsilon k_z \nabla_i \times (\mathbf{e}_z \rho z \cos\phi) + O(\epsilon^2)$$

and

$$\begin{aligned}\mathbf{B}_{ext} \;=\; & k_z \nabla_i (\rho \cos\phi) + i\epsilon \frac{k_x k_z}{4} \nabla_i \left(\rho^2 \cos(2\phi)\right) + i\epsilon \frac{k_x k_z}{4} \nabla_i \left(\rho^2 - 2z^2\right) \\ & + O\left(\epsilon^2\right),\end{aligned} \tag{46}$$

in the cylindrical coordinate variables.

Observing the form of the scalar potentials between (46) and those (15) in the TM incidence, we conclude that the first two terms are readily associated with the magnetic scalar potentials found in the

previous section, but with an additional incident factor k_z and with the triangular sine functions of the azimuthal angles replaced by the cosines. Trivial adjustments, e.g., the component orientations, are also needed for their conjugate vector potentials, and they can be found straightforwardly using the gauge condition. For brevity, they are not rederived here, and the solution in Table 1 holds (with the incident angle and directivity adjustment; see the caption).

The still unsolved potential is the first order magnetic scalar potential, $\Psi_M^{(1)}$, of the azimuthal mode $m = 0$. The integral equation that this potential satisfies is identical to (17) with $\Psi_{M,ext}^{(1)|^<} = ik_xk_z(\rho^2 - 2z^2)/4$, the zeroth aximuthal mode of the external incident field. The pore potential $\Psi_{M,pore}^{(1)}$ is expanded by

$$\Psi_{M,pore}^{(1)} = ik_xk_z\left(\bar{A}_{M,00}^{(1)} + \bar{A}_{M,0n}^{(1)}J_0(j'_{0n}\rho)\frac{\cosh(j'_{0n}(z+\ell))}{\cosh(j'_{0n}\ell)}\right), \quad (47)$$

and the inverted algebraic system for $\bar{A}_{M,00}^{(1)}$ and $\bar{A}_{M,0n}^{(1)}$ is referred to Appendix B. This leads to the second order inner electric vector potential in the form of

$$\begin{aligned}\mathbf{A}_{E,pore}^{(2)} = {} & \mathbf{e}_\rho D_n^{(2)} J_1(j'_{0n}\rho)\frac{\cosh(j'_{0n}(z+\ell))}{\cosh(j'_{0n}\ell)} \\ & + \mathbf{e}_z E_{0n}^{(2)} J_0(j'_{0n}\rho)\frac{\sinh(j'_{0n}(z+\ell))}{\cosh(j'_{0n}\ell)} + \mathbf{e}_z ik_xk_z\bar{A}_{M,00}^{(1)}(z+\ell), \quad (48)\end{aligned}$$

where $D_n^{(2)}$ and $E_n^{(2)}$ are the unknown coefficients to be solved. The last term arises due to the constant term $ik_xk_z\bar{A}_{M,00}^{(1)}$ in (47). The normal component of (48) is zero on the surface, which corresponds to the vanishing normal magnetic field on the perfect conducting surface. The radiation terms of the scalar and the vector potentials, including the magnetic scalar potential correction $\tilde{\Psi}_{M,sc}^{(4)}$ from the higher order, are

$$\begin{aligned}\Psi_{M,sc} &= -\epsilon^4\frac{k_xk_z}{6j'_{0n}}\bar{A}_{M,0n}^{(1)}\tanh(j'_{0n}\ell)J_2(j'_{0n})\big(1\text{–}3\cos^2\theta\big)h_2^{(1)}(S) \\ &\quad + \epsilon^4\tilde{\Psi}_{M,sc}^{(4)} = \epsilon^4\Psi_{M^{20},sc}^{(4)} + \epsilon^4\tilde{\Psi}_{M,sc}^{(4)}, \\ \tilde{\mathbf{A}}_{E,sc} &= -\epsilon^4\frac{iD_n^{(2)}}{2}\tanh(j'_{0n}\ell)J_2(j'_{0n})\sin\theta\begin{pmatrix}\cos\phi\\ \sin\phi\\ 0\end{pmatrix}h_1^{(1)}(S)\end{aligned}$$

$$+\epsilon^4 \frac{ik_x k_z}{2} \bar{A}^{(1)}_{M,00} \ell \cos\theta \begin{pmatrix} 0 \\ 0 \\ 1 \end{pmatrix} h^{(1)}_1(S) = \epsilon^4 \begin{pmatrix} \mathrm{A}^{(4)}_{E^{11}_x,sc} \\ \mathrm{A}^{(4)}_{E^{11}_y,sc} \\ \mathrm{A}^{(4)}_{E^{10}_z,sc} \end{pmatrix}.$$

They are all of $O(\epsilon^4)$. Applying the outer gauge condition, we obtain

$$D^{(2)}_n \tanh(j'_{0n}\ell) J_2(j'_{0n}) = -k_x k_z \bar{A}^{(1)}_{M,00}\ell + \frac{k_x k_z}{j'_{0n}} \bar{A}^{(1)}_{M,0n} \tanh(j'_{0n}\ell) J_2(j'_{0n}).$$

Interestingly, with the $D^{(2)}_n$, we find that the correction is a monopole,

$$\tilde{\Psi}^{(4)}_{M,sc} = \Psi^{(4)}_{M^{00},sc} = ik_x k_z \left(\frac{\bar{A}^{(1)}_{M,00}\ell}{2} - \frac{\bar{A}^{(1)}_{M,0n}}{3j'_{0n}} \tanh(j'_{0n}\ell) J_2(j'_{0n}) \right) h^{(0)}_0(S). \tag{49}$$

Its associated inner field is of $O(\epsilon^3)$, which we omit in this paper to proceed. One can, however, verify that the inner solution fulfills the Poisson equation $\nabla^2_i \Psi^{(3)} = -\Psi^{(1)}$, from $(11)_2$. Table 3 summarizes the radiation terms of this zero azimuthal mode, (49) and (49).

To illustrate the inner field of this mode, we use the same pore $\ell = 1.5$ and sketch the magnetic potential in Fig. 7. It is a quadrupole $(2, 0)$ field. The induced multipoles of this mode have a common incident factor $k_x k_z$. The contribution of these multipoles to the scattering field is, therefore, maximized when the incident angle is 45°. Their multipole moment coefficients, Fig. 8, however, exhibit a major different structure than those in Sections 3.3 and 3.4. The reason is the nonzero constant $\bar{A}^{(1)}_{M,00}$, Fig. 8(b), which leads to the moment

Table 3. Radiation of the zeroth azimuthal mode. These terms are in adjunct to those in Table 1 of the TE incidence.

Scalar electric potential	
$\Psi^{(4)}_{M^{20},sc} = k_x k_z \bar{B}^{(4)}_{M^{20}} h^{(1)}_2(S)(3\cos^2\theta - 1)$	$\bar{B}^{(4)}_{M^{20}} = \frac{1}{6j'_{0n}} \bar{A}^{(1)}_{M,0n} \tanh(j'_{0n}\ell) J_2(j'_{0n})$
$\Psi^{(4)}_{M^{00},sc} = ik_x k_z \bar{B}^{(4)}_{M^{00}} h^{(0)}_0(S)$	$\bar{B}^{(4)}_{M^{00}} =$ $\left(\frac{\bar{A}^{(1)}_{M,00}\ell}{2} - \frac{\bar{A}^{(1)}_{M,0n}}{3j'_{0n}} \tanh(j'_{0n}\ell) J_2(j'_{0n}) \right)$
Vector magnetic potential	Multipole moment coefficients
$\mathrm{A}^{(4)}_{E^{11}_x,sc} = ik_x k_z \bar{C}^{(4)}_{E^{11}} h^{(1)}_1(S) \sin\theta \cos\phi$	$\bar{C}^{(4)}_{E^{11}} =$ $\frac{1}{2} \left(\bar{A}^{(1)}_{M,00}\ell - \frac{\bar{A}^{(1)}_{M,0n}}{j'_{0n}} \tanh(j'_{0n}\ell) J_2(j'_{0n}) \right)$
$\mathrm{A}^{(4)}_{E^{11}_y,sc} = ik_x k_z \bar{C}^{(4)}_{E^{11}} h^{(1)}_1(S) \sin\theta \sin\phi$	
$\mathrm{A}^{(4)}_{E^{10}_z,sc} = ik_x k_z \bar{C}^{(4)}_{E^{00}} h^{(1)}_1(S) \cos\theta$	$\bar{C}^{(4)}_{E^{00}} = \frac{1}{2} \bar{A}^{(1)}_{M,00}\ell$

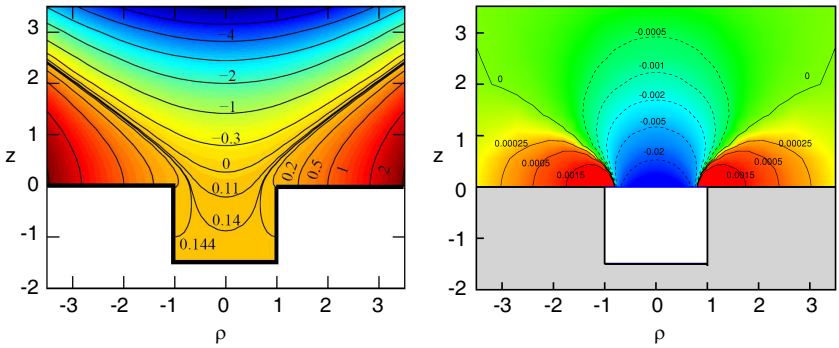

Figure 7. The additional magnetic scalar potential of the inner field for $\ell = 1.5$ for the TE incidence. The left is the total field. The right is the scattering multipole, $\Psi^{(1)}_{M,sc}$, after subtracting the external and the pore fields. It is the quadrupole $(2, 0)$. The fields are normalized by the incidence factors, which are 1 and ik_xk_z, respectively.

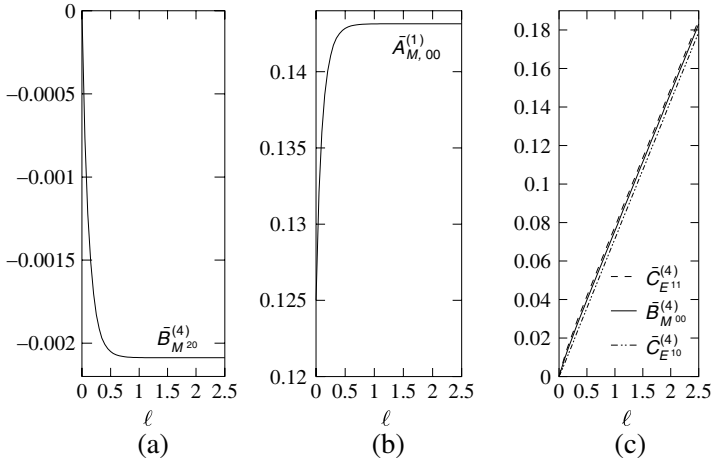

Figure 8. Multipole moment coefficients versus the pore depth, associated with the magnetic potentials of the TE incidence. (a) $\bar{B}^{(4)}_{M^{20}}$, (b) the constant $\bar{A}^{(1)}_{M,00}$ in (47), (c) coefficients with the effect of $\bar{A}^{(1)}_{M,00}$. For the finite thick plate, the horizontal axis is the plate thickness.

coefficients, $\bar{B}^{(4)}_{M^{00}}$, $\bar{C}^{(4)}_{E^{11}}$, and $\bar{C}^{(4)}_{E^{00}}$, being almost linearly proportional to the pore depth, Fig. 8(c). The dependence of these coefficients on ℓ contains the integrated effect of the depth-wise magnetic component of the TE polarized incidence.

As the previous section, we conclude here by presenting the explicit form of the leading order radiation of the physical fields, which reads

$$\begin{aligned}\mathbf{E}^{(3)}_{TE} &= \epsilon^3 k_z \bar{B}^{(2)}_{M^{11}} \frac{e^{iS}}{S} \begin{pmatrix} 0, \\ -\sin\phi, \\ -\cos\theta\cos\phi \end{pmatrix}_{\text{spherical}}, \\ \mathbf{B}^{(3)}_{TE} &= \epsilon^3 k_z \bar{B}^{(2)}_{M^{11}} \frac{e^{iS}}{S} \begin{pmatrix} 0, \\ \cos\theta\cos\phi, \\ -\sin\phi \end{pmatrix}_{\text{spherical}},\end{aligned} \tag{50}$$

with a linear dependence on k_z. The associated waveguide mode in the pore is a TE mode. It is simply the dipole field of (42) with a factor k_z, accounting for the horizontal component of the incident magnetic field, and with a rotation with respect to the z-axis by $-\pi/2$; i.e., $\phi \to \phi + \pi/2$.

5. LEADING DIPOLE RADIATION

The present method has been extended to find the scattering of a small pore in a finite thick perfect conducting plate; see the minimum details in [21]. Both reverse scattering and the transmitted waves are obtained. It is therefore informative to compare the dipoles between the two configurations, together with the classical dipole representations, Sections 11.1.2 and 11.1.3 [16].

The dipole radiation fields for both of TM and TE incidences read (42), (50) and (45). By aligning the magnetic and the electric dipole in the same way as in [21], we find that these dipoles are induced by the y- and x-, i.e., the horizontal, components of the incident magnetic field and the z-component of the incident electric field, respectively. Excluding the incident angle factors, 1, k_z and $-k_x$, the correspondent magnetic and electric dipole moments are

$$\mathbf{m} = 4\pi \bar{B}^{(2)}_{M^{11}}, \qquad \mathbf{p} = 4\pi \bar{B}^{(2)}_{E^{10}},$$

where the first magnetic dipole moment accounts for the two horizontal magnetic dipoles. Together with the reverse scattering and transmitted dipoles through the finite thick plate, we have the effective dipole moments versus the pore depth/plate thickness in Fig. 9.

Combining the two geometric configurations, we find that the reverse scattering asymptotes to the same strength, demonstrated by the leading dipoles, as the pore depth increases. The convergent manner versus the pore depth indicates that the source of the reverse scattering is localized near the pore exit facing towards the incident wave. The classical Bethe's solution, exactly at $|\mathbf{m}| = 8/3$ and $|\mathbf{p}| = 4/3$, [22], is also depicted for comparison.

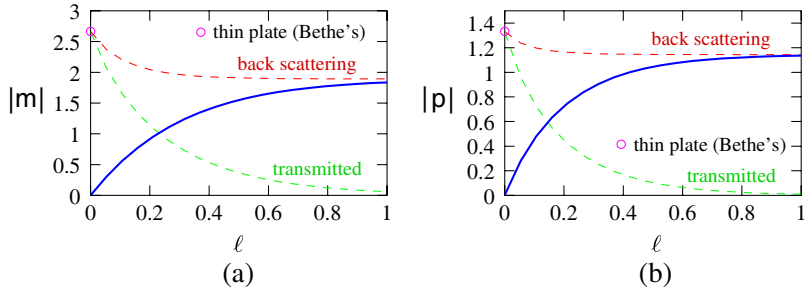

Figure 9. Comparison of the dipole moments to the back scattering and transmitted dipoles of the finite thick plate. (a) The magnetic dipole moment (b) the electrical dipole moment versus the pore depth (thick blue line).

6. CONCLUSION

The three-dimensional scattering wave field of electromagnetic waves incident obliquely on a small pore in a semi-infinite perfect conducting domain is solved analytically using the method of matched asymptotic expansion. In order to facilitate the analysis, we utilize the duality property of the source-free Maxwell equations to formulate the problem. This enables us to incorporate the solution found in a counterpart acoustic scattering problem, [17], to the electromagnetic wave system. In this formulation, an auxiliary scalar and a vector potential are introduced. Both the scalar and the vector potentials satisfy the wave equations if they satisfy the Lorentz gauge condition. When the pore is small, the wavelength is much larger than the radius of the pore, and therefore, the scattering field can be divided into an inner field, near the pore region, and an outer radiation field. Their characteristic length scales are the pore radius and the wavelength, respectively. The governing equations in the inner field can be simplified to the Laplace or Poisson equation. They are solved analytically by the method developed by Fabrikant. The outer radiation field is described by the wave equations and the scattering multipoles are determined by the matching procedures. With the help of the gauge condition, we carry out the matching procedure to $O(\epsilon)$ in the inner region and $O(\epsilon^4)$ in the outer region.

Both TM and TE polarized incident waves, as defined in Fig. 1, are calculated. For the two orders of the inner fields, the key for the solutions is the magnetic/electric scalar potentials, and five such fields, (20), (28), and (47), are found. The major contributors of the inner field are the two zeroth order fields, Figs. 3(a) and

5(a). They correspond somewhat to fields presented in [5] in the numerical investigation of the transmission of the electromagnetic waves through a rectangular hole. The electro/magneto-vector potentials are induced according to the gauge condition, and from their derived electro/magneto-fields in the pore, they are associated with TE and TM waveguide modes, respectively.

The inner fields lead to the radiation of the multipoles. By matching, we obtain multipole scattering expansions for both of the TM and TE polarized incident waves, which are summarized in Tables 1, 2, and 3. It is also found that, though the induced vector potentials in the inner region are one order smaller than the causing scalar potentials, there are components that radiate with the same order as the scalar potential radiation in the outer region. The physical electro/magneto-field radiation can only be correctly obtained by taking this mathematical structure into account.

In addition, the multipoles are not organized in a strictly ascending way. For example, in $O(\epsilon^4)$ of the radiation field, the scattering scalar potential waves are composed of octupoles, quadrupoles, and dipoles, and the vector potentials are composed of quadrupoles and dipoles, Tables 1 and 2. In the case of the TE incidence, there is even a monopole radiation of the magnetic scalar potential, Table 3, whose strength is linearly proportional to the depth of the pore. This does not mean that the monopole can exist alone; rather, in contrast, it has to be associated with its companion electric vector potential. This particular multipole structure is caused by the finite size effect of the pore.

The dependence of the incident angle is extracted as multiplier factors. The only geometric effect of the pore after normalization with respect to the pore radius is the depth. It modifies the wave scattering through its influence on the effective multipole moment coefficients, $\bar{B}^{(2,4)}_{ME^{mn}}$ and $\bar{C}^{(2,4)}_{EM^{mn}}$. The coefficients are shown to vanish altogether at $\ell = 0$. For TM incidence, the coefficients asymptote to their respective constant values when ℓ exceeds about 1. On the other hand, for TE incidence, the magnetic component in the depth-wise direction induces radiation multipoles of $O(\epsilon^4)$, whose strengths are linearly proportional to the pore depth. The incident factors also reveal the alternation of the induced waveguide modes in the pore. When the wave is normally shed on the pore, $k_x = 0$, only the TE mode in the pore is excited. When the incident wave is inclined with a non-zero z-component of the electric field, the TM waveguide mode is raised.

The leading dipole fields for both of the incident polarizations are explicitly calculated. For the magnetic scalar potential, the dipole lies on the horizontal xy plane, but for the electric scalar potential,

the dipole is vertical to the pore exit. The present theory has been extended to the scattering of a small pore in a finite thick perfect conducting plate. Both reverse scattering and the transmitted waves are obtained. Combining the two results, we find that the reverse scattering asymptotes to the same strength, demonstrated by the leading dipoles, as the pore depth increases. The fast convergence versus the pore depth indicates that the source of the reverse scattering is localized near the pore exit facing towards the incident wave. The classical Bethe's solution, [22], is also depicted for comparison between the two geometric configurations. In the future, the present expansions will enable us to treat the pore as an individual scatterer and thus to investigate the wave fields from surfaces with various pore structures by formulating the mutual interactions as multiple scattering processes; see Garcia de Abajo [3], Ishimaru [23].

ACKNOWLEDGMENT

This work is supported in part by grant NSC-97-2221-E-001-023-, Taiwan, Republic of China.

APPENDIX A. ALGEBRAIC EQUATIONS FOR TM INCIDENCE

We use the method developed by Fabrikant, [18], to find analytically the asymmetric three-dimensional potentials. The solving procedures are detailed in [17] and are not repeated here. For the zeroth order, we have the electric potential, $\Psi_E^{(0)}$, analogous to the acoustic wave with the pressure-release condition and the magnetic potential, $\Psi_M^{(0)}$, to that with the rigid wall condition. The inverted algebraic systems for the integral equations of the two potentials, (26) and (17), are accordingly

$$\mathbf{M}_M^{(0,1)}\mathbf{A}_{M,1}^{(0,1)} = \mathbf{N}_M^{(0,1)}, \qquad \mathbf{M}_E^{(0,1)}\mathbf{A}_{E,0}^{(0,1)} = \mathbf{N}_E^{(0,1)}, \tag{A1}$$

For the former equation, we have the vectors and the matrices

$$\mathbf{N}_M^{(0)} = \frac{2}{j_{1l}'^2}\left(\sin j_{1l}' - j_{1l}'\cos j_{1l}'\right),$$
$$\mathbf{N}_M^{(1)} = ik_x\frac{2}{3}\sqrt{\frac{\pi}{2j'_{2n}}}J_{\frac{5}{2}}(j'_{2n}),$$

$$\mathbf{M}_M^{(0,1)} = \begin{cases} \frac{\pi}{2}\left\{\frac{j'_{ml}}{2}\left(J^2_{m+\frac{1}{2}}(j'_{ml}) - J_{m-\frac{1}{2}}(j'_{ml})\,J_{m+\frac{3}{2}}(j'_{ml})\right)\right. \\ \qquad \left. + J_{m+\frac{1}{2}}(j'_{ml})\,J_{m-\frac{1}{2}}(j'_{ml})\right\} \\ \qquad + \frac{\pi}{4} j'_{ml}\tanh(j'_{ml}\ell)\left(1 - \frac{m^2}{j'^2_{ml}}\right) J^2_m(j'_{ml}) & \text{if } n = l, \\ \\ \frac{\pi}{2}\frac{(j'_{mn}j'_{ml})^{-1/2}}{j'^2_{mn} - j'^2_{ml}}\left\{j'^2_{mn} j'_{ml} J_{m+\frac{1}{2}}(j'_{mn})\,J_{m-\frac{1}{2}}(j'_{ml})\right. \\ \qquad \left. - j'_{mn} j'^2_{ml} J_{m-\frac{1}{2}}(j'_{mn}) J_{m+\frac{1}{2}}(j'_{ml})\right\} & \text{if } n \neq l, \end{cases} \tag{A2}$$

where $m = 1$ and 2 for $\mathbf{M}_M^{(0)}$ and $\mathbf{M}_M^{(1)}$, respectively. On the other hand, the vectors and the matrices of $(\mathrm{A1})_2$ read

$$\mathbf{N}_E^{(0)} = -k_x\sqrt{\frac{2}{\pi}}\, j_{0l}^{-\frac{3}{2}} J_{\frac{3}{2}}(j_{0l}),$$

$$\mathbf{N}_E^{(1)} = -ik_x^2\frac{2}{3}\sqrt{\frac{2}{\pi}}\, j_{1n}^{-\frac{3}{2}} J_{\frac{5}{2}}(j_{1n}),$$

$$\mathbf{M}_E^{(0,1)} = \begin{cases} -\frac{1}{2j_{ml}}\tanh(j_{ml}\ell) J_{m-1}(j_{ml}) J_{m+1}(j_{ml}) \\ \quad + \frac{1}{2j_{ml}}\left\{J^2_{m+\frac{1}{2}}(j_{ml}) - J_{m-\frac{1}{2}}(j_{ml}) J_{m+\frac{3}{2}}(j_{ml})\right\}, & \text{if } n = l, \\ \\ \frac{(j_{mn}j_{ml})^{-1/2}}{j^2_{mn} - j^2_{ml}}\left\{j_{ml} J_{m+\frac{1}{2}}(j_{mn}) J_{m-\frac{1}{2}}(j_{ml})\right. \\ \quad \left. - j_{mn} J_{m-\frac{1}{2}}(j_{mn}) J_{m+\frac{1}{2}}(j_{ml})\right\}, & \text{if } n \neq l, \end{cases}$$

with $m = 0$ and 1 for $\mathbf{M}_E^{(0)}$ and $\mathbf{M}_E^{(1)}$, respectively.

APPENDIX B. ALGEBRAIC EQUATIONS FOR TE INCIDENCE

For the first order scalar potential of the azimuthal mode $m = 0$ in the pore, (47), we have the inverted algebraic system

$$\begin{pmatrix} 1 & \mathbf{V}^T \\ \mathbf{V} & \mathbf{M}_M^{(1)} \end{pmatrix} \begin{pmatrix} A_0^{(1)} \\ \mathbf{A}_0^{(1)} \end{pmatrix} = ik_x k_z \begin{pmatrix} \frac{1}{6} \\ \mathbf{N}_M^{(1)} \end{pmatrix},$$

where the sub-matrices and vectors are

$$\begin{aligned} \mathbf{A}_0^{(1)} &= A_{0l}^{(1)}, \\ \mathbf{V} &= V_n = \frac{\sin(j'_{0n})}{j'_{0n}}, \\ \mathbf{N}_M^{(1)} &= N_{M,l}^{(1)} = \frac{(j'^2_{0l} - 2)\sin j'_{0l} + 2j'_{0l}\cos j'_{0l}}{2j'^3_{0l}}, \end{aligned}$$

and

$$\mathbf{M}_M^{(1)} = \begin{cases} \frac{1}{2}\left(1+\frac{\sin(2j'_{0n})}{2j'_{0n}}\right) + \frac{\pi j'_{0n}}{4}\tanh(j'_{0n}\ell)J_0^2(j'_{0n}), & \text{if } n=l, \\ \frac{1}{2}\left(\frac{\sin(j'_{0n}-j'_{0l})}{j'_{0n}-j'_{0l}} + \frac{\sin(j'_{0n}+j'_{0l})}{j'_{0n}+j'_{0l}}\right), & \text{if } n\neq l. \end{cases}$$

REFERENCES

1. Pendry, J. B., L. Martin-Moreno, and F. J. Garcia-Vidal, "Mimicking surface plasmons with structured surfaces," *Science*, Vol. 305, 847–848, 2004.
2. Garcia de Abajo, F. J. and J. J. Saenz, "Electromagnetic surface modes in structured perfectconductor surfaces," *Phys. Rev. Lett.*, Vol. 95, No. 4, 233901, 2005.
3. Garcia de Abajo, F. J., "Colloquium: Light scattering by particle and hole arrays," *Rev. Mod. Phys.*, Vol. 79, 1267–1290, 2007.
4. Garcia de Abajo, F., "Light transmission through a single cylindrical hole in a metallic film," *Opt. Express*, Vol. 10, No. 25, 1475–1484, 2002.
5. Garcia-Vidal, F. J., E. Moreno, J. A. Porto, and L. Martin-Moreno, "Transmission of light through a single rectangular hole," *Phys. Rev. Lett.*, Vol. 95, 103901, 2005.
6. Stevenson, A. F., "Electromagnetic scattering by an ellipsoid in the third approximation," *J. Appl. Phys.*, Vol. 24, 1143–1151, 1953.
7. Stevenson, A. F., "Solution of electromagnetic scattering problems as power series in the ratio (dimension of scatterer)/wavelength," *J. Appl. Phys.*, Vol. 24, 1134–1142, 1953.
8. Lee, J. G. and H. J. Eom, "Magnetostatic potential distribution through a circular aperture in a thick conducting plane," *IEEE Trans. Electromagn. Compat.*, Vol. 40, 97–99, 1998.
9. Lee, J. H. and H. J. Eom, "Electrostatic potential through a circular aperture in a thick conducting plane," *IEEE Trans. Micro. Theory Tech.*, Vol. 44, 341–343, 1996.
10. Hansen, T. B. and A. D. Yaghjian, "Low-frequency scattering from two-dimensional perfect conductors," *IEEE Trans. Ant. Prop.*, Vol. 40, 1389–1402, 1992.
11. Scharstein, R. W. and A. M. J. Davis, "Matched asymptotic expansion for the low-frequency scattering by a semi-circular trough in a ground plane," *IEEE Trans. Ant. Prop.*, Vol. 48, 801–811, 2000.
12. Butler, C. M., Y. Rahmat-Samii, and R. Mittra, "Electromagnetic

penetration through apertures in conducting surfaces," *IEEE Trans. Ant. Prop.*, Vol. 26, 82–93, 1978.

13. Cwik, T. A. and R. Mittra, "Scattering from a periodic array of free-standing arbitrarily shaped perfectly conducting or resistive patches," *IEEE Trans. Ant. Prop.*, Vol. 35, 1226–1234, 1987.
14. Roberts, A., "Electromagnetic theory of diffraction by a circular aperture in a thick, perfectly conducting screen," *J. Opt. Soc. Am. A*, Vol. 4, No. 10, 1970–1983, 1987.
15. Roberts, A., "Near-zone fields behind circular apertures in thick, perfectly conducting screens," *J. Appl. Phys.*, Vol. 65, 2896–2899, 1989.
16. Griffiths, D. J., *Introduction to Electrodynamics*, 416–476, Prentice Hall, 1999.
17. Kuo, C. Y., R. L. Chern, and C. C. Chang, "Sound scattering by a compact circular pore," *J. Sound Vib.*, Vol. 319, 2009.
18. Fabrikant, V. I., *Applications of Potential Theory in Mechanics, a Selection of New Results*, Kluwer, 1989.
19. Crighton, D. G., A. P. Dowling, J. E. Ffowcs Williams, M. Heckl, and F. G. Leppington, *Modern Methods in Analytical Acoustics*, Chap. 13, 168–208, Springer-Verlag, 1992.
20. Morse, P. M. and H. Feshbach, *Methods of Theoretical Physics*, Part 2, Chap. 13, McGraw-Hil, 1953.
21. Chern, R. L., C. Y. Kuo, H. W. Chen, and C. C. Chang, "Electromagnetic scattering by a subwavelength circular hole in a perfect metal plate of finite thickness: Matched asymptotic expansion," *J. Opt. Soc. Am. B*, Vol. 27, 1031–1043, 2010.
22. Bethe, H. A., "Theory of diffraction by small holes," *Phys. Rev.*, Vol. 66, 163–182, 1944.
23. Ishimaru, A., *Wave Propagation and Scattering in Random Media*, IEEE, 1994.